Geothermobarometry in 4-Phase Lherzolites .1. Experimental Results from 10 to 60 Kb

Article *in* Journal of Petrology · December 1990

DOI: 10.1093/petrology/31.6.1313

CITATIONS
195

READS
549

3 authors, including:

Gerhard Peter Brey
Goethe-Universität Frankfurt am Main
234 PUBLICATIONS **9,539** CITATIONS

SEE PROFILE

K.G. Nickel
University of Tuebingen
265 PUBLICATIONS **4,499** CITATIONS

SEE PROFILE

0022-3530/90 $3.00

Geothermobarometry in Four-phase Lherzolites I. Experimental Results from 10 to 60 kb

by G. P. BREY[1], T. KÖHLER[1] AND K. G. NICKEL[1,2]

[1]*Max-Planck-Institut für Chemie, Abt. Kosmochemie, Saarstr. 23, D-6500 Mainz, West Germany*

[2]*Max-Planck-Institut für Metallforschung, Abt. Pulvermetallurgie, Heisenbergstr. 17, D-7000 Stuttgart, West Germany*

(*Received 26 September 1989; revised typescript accepted 15 May 1990*)

ABSTRACT

Experiments were carried out on primitive natural lherzolitic compositions from 10 to 60 kb and 900 to 1400 °C. Mineral compositions were reversed by using mixes of finely ground ($<20\ \mu m$) minerals from natural rock samples with different initial compositions. The minerals were mixed in proportions to give a primitive upper mantle composition. Further starting materials were a synthetic mineral mix and a sintered oxide mix. Equilibrium was thus approached from different chemical directions, and equilibrium mineral compositions were inferred from the overlap of microprobe analyses. Fe-loss problems were avoided by using single-crystal olivines as sample containers. Samples were placed into holes drilled into cylindrically shaped olivine crystals, which in turn were welded into Pt capsules. A further advantage of this method is that oxygen fugacities seem to be buffered by the Ni precipitation curve. This curve lies very close to the iron–wüstite (IW) buffer curve for mantle olivines. Oxygen fugacities calculated from compositions of experimentally produced spinels give values slightly above the IW buffer curve. Therefore, practically no Fe^{3+} should be present in our experimental charges.

Ortho- and clinopyroxene compositions were strictly reversed with respect to Al, Cr, and Na (only cpx) contents and their mutual amounts of enstatite and diopside components. The data show the fundamental influence of Na in cpx on two-pyroxene thermometry. Garnet compositions were reversed with respect to Ca, Al, Cr, Ti, and Mn. Other than in CMAS, Ca in garnet is mostly dependent on temperature in the natural system and not so much on pressure. This behaviour of Ca will most strongly influence barometers based on the Al content of orthopyroxene coexisting with garnet. The *mg*-numbers of coexisting phases were not strictly reversed. The homogeneity of olivine compositions and internal consistency of the data set give us confidence that equilibrium values of *mg*-number have been reached in almost all cases. The experimental results presented in this paper offer the unique possibility of simultaneously testing many different thermobarometers which are based on different exchange reactions and which were calibrated in different laboratories.

INTRODUCTION

Spinel and garnet peridotites occurring as xenoliths in kimberlites and other volcanic rocks and in alpine-type peridotite bodies are a major source of information about the physical and chemical properties and processes of the upper mantle. The use of mineral chemistry to give estimates of pressures and temperatures of crystallization of these rocks has been an important tool to gain such information since the pioneering study of Boyd (1973). Ever since Boyd's work there has been debate on the correct extrapolation of experimental results in simple systems to natural rocks and to P, T conditions not covered by experiments. Also, systematic errors in either calculated pressure or temperature result in increased errors of the other parameter because of positively correlated correction terms for pressure and temperature in existing thermometers and barometers.

Wood & Banno (1973) made the first comprehensive attempt to correct experimental results in the simple systems CaO–MgO–SiO_2 (CMS) and MgO–Al_2O_3–SiO_2 (MAS) by thermodynamic modelling for non-CMS and non-MAS components. This resulted in the combined application of the two-pyroxene thermometer (CMS; based on the exchange of enstatite component between coexisting ortho- and clinopyroxene) and the Al-in-opx barometer (MAS; based on Al content of orthopyroxene coexisting with garnet). The widely used Wells (1977) thermometer and the Nickel & Green (1985) barometer are updated versions of these.

Finnerty & Boyd (1984, 1987) used an empirical fit to diopside compositions from reversed experiments on coexisting ortho- and clinopyroxene in the simple CMS system as a thermometer. They combined this thermometer with a barometer based on Al_2O_3-isopleths in opx (wt.%) from experiments by MacGregor (1974) in the simple MAS system. This combination of a thermometer and a barometer is the only one which places the diamond-bearing lherzolite xenolith BD 2125 (Dawson & Smith, 1975) into the diamond stability field and the primary graphite-bearing xenolith PHN 1569 (Nixon & Boyd, 1973) into the graphite stability field (graphite–diamond reaction boundary taken from Kennedy & Kennedy, 1976). Carswell & Gibb (1987*a*) noted, however, that use of the graphite–diamond boundary to test the accuracy of thermobarometers is rather weak, mainly because the test applies to a single P, T condition with no test for other pressures and temperatures. Several other combinations of a thermometer and barometer place BD 2125 close enough to the graphite–diamond boundary to yield satisfactory agreement with the phase diagram within the stated errors.

Carswell & Gibb (1987*a*, 1987*b*) followed a rather different approach and used available experimental results in natural peridotitic systems to test existing thermometers and barometers. They concluded that the use of an average temperature calculated with the Bertrand & Mercier (1985) two-pyroxene thermometer and various Fe–Mg exchange thermometers in combination with the Al-in-opx-barometer of Nickel & Green (1985) best reproduced the experimental data. Currently available experiments in natural systems are hampered by (1) the lack of reversed experiments, i.e., demonstrated equilibrium by the use of different types of starting materials but, rather, inferred equilibrium from 'homogeneity' of the run products, (2) short run times, (3) loss of Fe to noble metal capsules, and (4) poor-quality microprobe analyses. On these grounds, Carswell & Gibb (1987*a*, 1987*b*) considered the experiments of Akella (1976) and Nickel (1983) to be the most satisfactory. They noted considerable reservations towards the experiments of Mori & Green (1978), and rejected those of Kushiro *et al.* (1972) and Green (1973).

Bertrand & Mercier (1985) and Bertrand *et al.* (1986) tested a newly developed thermometer and barometer with the experimental data sets of Akella (1976) and Mori & Green (1978) on natural systems, and found satisfactory reproduction of experimental conditions. Their thermometer is based on results from the CMS system with a theoretical correction for Na in both pyroxenes and an empirical correction of Ca in clinopyroxene for Fe from the CaO–FeO–MgO–SiO_2 (CFMS) system. The barometer is based on the MAS system with an empirical correction for Fe in garnet from the FeO–MgO–Al_2O_3–SiO_2 (FMAS) system and a pressure-dependent correction term for Ca in garnet from the CaO–MgO–Al_2O_3–SiO_2 (CMAS) system.

Both the approach by Carswell & Gibb (1987*a*, 1987*b*) and that of Bertrand & Mercier (1985) and Bertrand *et al.* (1986) suffer from the shortcomings of the experimental data set in the natural system, i.e., mineral compositions are not demonstrated to be in equilibrium, and loss of Fe to noble metal capsules. Also, the experiments in the natural systems were carried out over a restricted range of pressures (mostly 30–40 kb) with application to rocks

from up to 70 kb. We have therefore embarked on an experimental study with natural lherzolitic compositions from 10 to 60 kb and 900 to 1400 °C, where mineral compositions were reversed and the Fe-loss problem is avoided.

EXPERIMENTAL METHODS

Single-crystal olivines were used as sample containers to circumvent the Fe-loss problem (Fig. 1). The olivines (*mg*-number from 89 to 91) from San Carlos, AZ, were embedded into epoxy resin, cut to the desired height of the capsule (4 mm) and the cylinders were cored with a diamond drill. Similarly, 1-mm discs were cut from olivines to serve as capsule lids. Up to four different starting materials could be used simultaneously by placing them in different holes drilled into one cylinder (Fig. 1). The holes were closed with the olivine lids and the containers were welded into thick-walled (0·2-mm) Pt containers (the large amount of Pt keeps the temperature gradient within the capsule to < 10 °C; Brey *et al.*, in press). This method has the further advantage that all different starting materials are subjected to *identical P, T* conditions. Depending on pressure, temperature, and time, restricted Fe loss from the olivine capsule to the Pt container occurs by diffusion over up to 100 μm where the olivine appears to remain a single crystal as seen in reflected light (Fig. 2a). Fe loss occurs over up to 300 μm where the olivine capsule recrystallized during the experiment (Fig. 2b). The distance between the sample holes and Pt wall was always > 700 μm. Because of the similarity of compositions of olivine capsules and of bulk *mg*-numbers of the starting

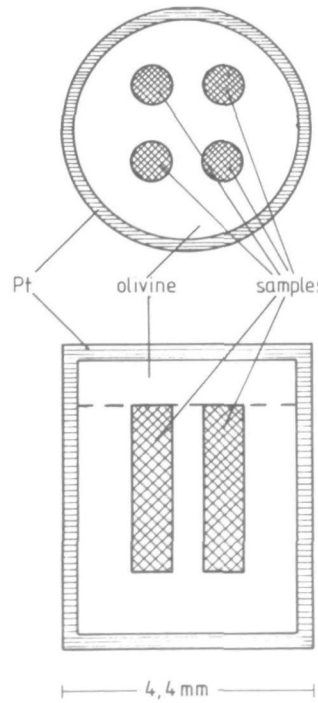

FIG. 1. Sample capsule for experiments with natural lherzolitic compositions. Up to four holes were drilled into single-crystal olivine cylinders so that four different starting materials could be run simultaneously. The holes were covered with an olivine lid and everything was welded into Pt tubing with 0·2-mm wall thickness.

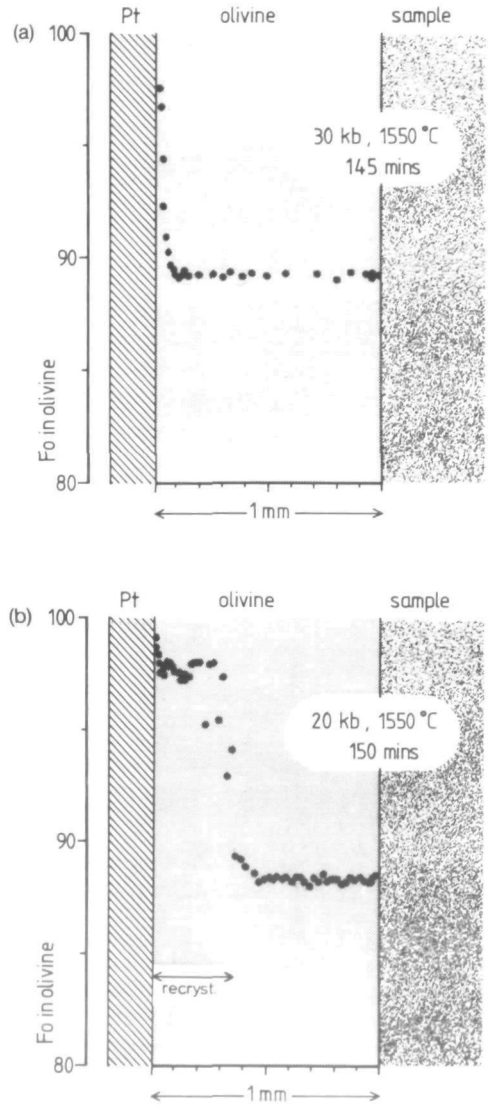

FIG. 2. (a) Fe loss profile (as Fo content) at the rim of the olivine cylinder to the Pt wall where olivine appears as an intact single crystal in reflected light. The examples here and in (b) are taken from an unpublished project on partitioning of Ni and Co between olivine and metal melt. These examples are chosen to demonstrate extreme cases of Fe loss at very high temperatures. Each dot represents a microprobe analysis. Fe loss occurs over $\sim 100\ \mu m$, seemingly by volume diffusion. (b) Fe loss to Pt where olivine recrystallized during the experiment to a fine olivine aggregate with 120° angles between the grains. Fe loss is much more extensive, probably because of grain boundary diffusion.

materials (Table 1), the Fe content of starting materials did not change during an experiment.

Experiments from 10 to 28 kb were carried out in a Boyd and England-type piston cylinder apparatus. Cold-pressed NaCl was used as pressure-transmitting medium at all temperatures except for runs P6 and P17 (see Table 2), for which we used cold-pressed, hot-sintered CaF_2 (93% theoretical density, courtesy V. Bulatov, Institute of Lithosphere,

TABLE 1

Composition of minerals (in wt.%) in different starting materials and bulk composition of spinel lherzolite SC-1 (from Jagoutz et al., *1979)*

SC-1	*bulk*	*ol*	*opx*	*cpx*	*sp*
SiO_2	45·1	40·42	54·71	51·51	0·53
TiO_2	0·22	—	0·26	0·66	0·32
Al_2O_3	4·14	—	5·30	7·52	58·86
Cr_2O_3	0·45	—	0·36	0·73	8·33
FeO	7·82	9·58	6·13	3·24	10·94
MnO	—	—	0·15	0·10	0·09
NiO	—	0·32	0·11	0·045	0·42
MgO	38·00	48·99	31·87	14·81	20·23
CaO	3·54	—	0·96	19·78	—
Na_2O	0·36	—	0·15	1·58	—
Sum	99·63	99·31	99·85	99·98	99·72
mg-number	89·65	90·1	90·3	89·1	76·72
Mo22		*ol*	*opx*	*cpx*	*sp*
SiO_2		40·85	54·59	51·85	—
TiO_2		—	0·14	0·46	0·2
Al_2O_3		—	5·55	6·93	57·85
Cr_2O_3		—	0·44	0·78	10·40
FeO		10·05	6·17	3·58	8·84
MnO		—	0·13	—	—
NiO		0·35	—	—	—
MgO		48·80	31·75	15·45	21·38
CaO		—	0·99	18·70	—
Na_2O		—	—	1·53	—
Sum		100·05	99·75	99·27	100·71
mg-number		89·6	90·15	88·48	81·17
	grt Baro	*J4: ol*	*opx*	*cpx*	*grt*
SiO_2	41·65	40·47	57·78	55·21	41·64
TiO_2	1·08	—	—	0·30	0·70
Al_2O_3	21·36	—	1·03	3·04	21·28
Cr_2O_3	2·25	—	0·20	0·91	2·04
FeO	—	10·26	6·34	4·31	7·88
MnO	0·67	—	—	—	0·27
NiO	—	0·41		—	—
MgO	13·69	48·90	33·54	17·88	21·42
CaO	19·30	—	0·90	15·85	4·24
Na_2O		—	0·20	2·34	—
Sum	100·00	100·04	99·75	100·00	99·47
mg-number		89·6	88·90	88·10	82·90

Mineral analyses in SC-1 are from Blum *et al.* (1982), for spinel lherzolite Mo22 from Preß *et al.* (1986), and our own analyses for garnet lherzolite J4.

Moscow). This type of 'low-friction-cell' requires no pressure correction for friction loss (e.g., Mirwald *et al.*, 1975; V. Bulatov, pers. comm., 1988). Nominal pressure was taken as the pressure on the sample, and was controlled to within 250 b.

Experiments at 30 kb and above were carried out with a belt-type apparatus commercially available from Pressure Systems Research, Pleasanton, CA. The pressure-transmitting solid media consisted mostly of polycrystalline natural CaF_2, with factory-processed pyrophyllite as gasket material. Pressure was calibrated at room temperature with

TABLE 2

Midpoints of experimental brackets or selected values from diagrams of type Figs. 3–5 inferred to represent equilibrium compositions

P5: 10 kb, 1000 °C; 114 h; $H_2O = 5\%$; ol, opx, cpx, sp, L; EDS

	ol	*opx*	*cpx*		*sp*	*sp*
Ca		0·030	0·870	Mg	5·822	5·567
Al		0·097	0·165	Al	8·502	8·946
Cr		0·018	0·029	Cr	7·305	6·784
Na			0·015	V	0·025	0·045
Ti			0·0025	Ti	0·038	0·077
				Fe^{2+}	2·220	2·514
				Fe^{3+}	0·089	0·067
Nor	91·6	92·2	93·0		71·6	
Kola	89·5	90·3	90·6			68·3

P12: 10 kb, 1100 °C; H_2O = br.; ol, opx, cpx, sp, L; WDS

	ol	*opx*		*cpx*	
Ca		0·050	(0·035–0·056)	0·770	(0·740–0·820)
Al		0·180	(0·168–0·190)	0·250	(0·217–0·285)
Cr		0·014	(0·010–0·017)	0·020	(0·014–0·027)
Na				0·042	(0·024–0·060)
Ti		0·004		0·014	(0·007–0·02)
Kola	87·6	88·8		88·8	
J4	89·2	90·0		90·1	
Nor	91·6	91·3		92·5	
Baro	92·0	93·2		93·1	

sp	*Mg*	*Al*	*Cr*	*Ti*	Fe^{2+}	Fe^{3+}
Kola	6·256	12·800	2·834	0·023	1·769	0·318
Nor	6·774	14·444	1·462	0·017	1·236	

P17: 15 kb, 1100 °C; 70 h; H_2O = br.; ol, opx, cpx, sp, L; EDS

	ol	opx		cpx	
Ca		0·045	(0·038–0·045)	0·796	
Al		0·190	(0·173–0·200*)	0·222	(0·205–0·240)
Cr(J4)		0·020		0·036	
Cr		0·013		0·026	
Na(J4)				0·045	
Na				0·030	
Ti				0·008	
Nor	90·6	90·7		90·5	
J4	88·7	89·5		89·6	
Kola	88·0	89·3		88·5	
Baro	91·0	91·7		92·0	

P28: 21 kb, 1000 °C; 168·5 h; H_2O = 5%; ol, opx, cpx, sp, L; EDS

	ol	opx		cpx	
Ca		0·026	(0·023–0·030)	0·862	(0·845–0·868)
Al		0·151	(0·144–0·158)	0·165	(0·144–0·175)
Cr		0·017	(0·014–0·020)	0·025	(0·018–0·029)
Cr (J4)		0·021		0·031	
Na				0·026	(0·022–0·035)
Na(J4)				0·033	
Ti				0·005	
Nor	91·5	91·6		92·7	
J4	91·5	90·4		91·3	
Kola	92·0	90·4		91·3	

P8: 20 kb, 1100 °C; 72 h; H_2O = 1%; ol, opx, cpx, sp, L; EDS

	ol	opx		cpx	
Ca		0·041	(0·037–0·044)	0·773	
Al		0·215	(0·203–0·236)	0·258	(0·251–0·264)
Cr		0·020	(0·018–0·023)	0·036	(0·031–0·041)
Na				0·085	(0·065–0·093)
Ti				0·005	
Nor	92·6	92·7		93·0	
J4	91·3	91·2		91·2	
Kola	90·0	89·9		90·1	
Baro	91·8	92·9		92·7	

TABLE 2 (*Continued*)

P6: 20 kb, 1200°C; 13·75 h; H_2O = br.; ol, opx, cpx, sp, L; EDS

	ol	*opx*	*cpx*
Ca		0·063	0·736
Al		0·144	0·154
Cr		0·027	0·036
Na			0·031
Kola	87·6	88·4	88·5

J4: ol, opx, L; NOR: ol, opx (no good analyses), cpx, L; Baro: ol, opx, cpx, sp, L; values above only from Kola

P2: 28 kb, 1000°C; 144 h; H_2O ≈ 5%; ol, opx, cpx, grt; EDS

	ol	*opx*		*cpx*		*grt*	
Ca		0·023	(0·022–0·024)	0·825	(0·804–0·832)	0·137	*(0·137–0·125)
Al		0·080	(0·079–0·091)	0·129	(0·124–0·134)	1·815	(1·785–1·845)
Cr		0·012	(0·012–0·013)	0·031	(0·028–0·034)	0·124	(0·117–0·130)
Na				0·079	(0·068–0·090)		
Ti						0·009	
Mn						0·020	*(0·020–0·015)
J4	89·2	90·3		92·0		81·3	
SC-1	89·2	90·3		92·0		81·3	

P3: 28 kb, 1150°C; 20 h; H_2O = br.; ol, opx, cpx, grt; EDS

	ol	*opx*		*cpx*		*grt*	
Ca		0·040	(0·035–0·042)	0·776	(0·746–0·786)	0·147	*(0·139–0·155)
Al		0·128	(0·122–0·136)	0·154	(0·143–0·158)	1·795	(1·755–1·835)
Cr		0·017	(0·013–0·022)	0·034	(0·028–0·039)	0·145	(0·125–0·165)
Na				0·065	(0·054–0·076)		
Ti						0·011	(0·009–0·013)
Mn						0·013	(0·011–0·015)
J4	90·1	90·8		90·8		82·8	
SC-1	90·1	90·8		90·8		82·8	

P21: 31 kb, 900°C; 282·5 h; $H_2O = 5\%$; ol, opx, cpx, grt; EDS

	ol	opx	cpx		grt	
Ca		0·015	0·854		0·155	*(0·145–0·166)
Al		0·052	0·100	(0·088–0·110)	1·788	(1·745–1·830)
Cr		0·008	0·035	(0·021–0·038)	0·125	(0·110–0·140)
Na			0·070	(0·060–0·080)		
Ti					0·015	(0·010–0·018)
Mn					0·030	(0·020–0·030)
Kola	88·9	89·6	91·9		76·7	
Baro	92·2	93·5	94·0		85·8	
Nor	91·8	91·8	94·0		82·7	
J4	89·8	90·5	92·3		78·4	

472: 30 kb, 1000°C; 144·15 h; $H_2O = 2{\cdot}5\%$; ol, opx, cpx, grt; EDS

	ol	opx	cpx		grt	
Ca		0·021	(0·018–0·023)	0·830	(0·820–0·830)	0·139	*(0·134–0·143)
Al		0·067	(0·059–0·075)	0·092		1·868	(1·84–1·895)
Al(J4)				0·103			
Cr		0·010	(0·008–0·012)	0·019		0·125	
Cr(J4)				0·031			
Na				0·072	(0·067–0·075)		
Na(J4)				0·090			
Ti				0·0025		0·012	
Mn						0·024	
Kola	88·1	88·9		90·1		77·4	
J4	88·4	89·2		90·2		78·0	
Nor	88·6	90·0		91·5		78·5	

458: 30 kb, 1100°C; 68 h; $H_2O = 2{\cdot}5\%$; ol, opx, cpx, grt; EDS

	ol	opx	cpx		grt	
Ca		0·030	(0·026–0·035)	0·810	(0·805–0·818)	0·148	*(0·141–0·155)
Al		0·104	(0·089–0·119)	0·136	(0·130–0·142)	1·855	(1·82–1·900)
Cr		0·014	(0·009–0·018)	0·033	(0·027–0·036)	0·125	(0·080–0·130)
Na				0·070			
Ti						0·008	(0·005–0·011)
Mn						0·018	(0·014–0·022)
Nor	89·9	91·5		91·6		82·1	
Meym	89·5	89·8		90·5		81·0	
J4	89·5	89·8		90·5		81·0	

TABLE 2 (*Continued*)

466: 30 kb, 1200°C; 27 h; H_2O = br.; ol, opx, cpx, grt; EDS							
	ol	*opx*		*cpx*		*grt*	
Ca		0·045		0·750		0·140	
Al		0·130		0·160		1·84–1·9	
Cr		0·017	(0·013–0·020)	0·030	(0·026–0·033)	0·125	(0·100–0·150)
Na				0·063	(0·058–0·076)		
Ti				0·06	(0·000–0·012)	0·014	
Mn						0·019	
Nor	90·7	91·0		90·8		85·2	
Meym	89·3	89·6		88·8		82·0	
J4:	no cpx						
467: 30 kb, 1300°C; 4·5 h; H_2O = abs.; ol, opx, cpx, grt; EDS							
	ol	*opx*		*cpx*		*grt*	
Ca		0·065	(0·061–0·069)	0·640	(0·610–0·668)	0·137	*(0·135–0·139)
Al		0·162	(0·153–0·172)	0·195	(0·187–0·222)	1·85	(1·8–1·9)
Cr		0·020	(0·016–0·025)	0·025	(0·022–0·029)	0·120	(0·100–0·130)
Na		0·010	(0·005–0·018)	0·065	(0·055–0·085)		
Ti						0·010	(0·000–0·017)
Mn						0·015	
J4	89·4	90·0		89·0		83·5	
Nor	90·7	91·8		91·3		86·6	
Kola	88·3	89·0		88·0		82·4	
500: 40 kb, 900°C; 311 h; H_2O = 5%; ol, opx, cpx, grt, EDS							
	ol	*opx*		*cpx*		*grt*	
Ca		0·010	(0·006–0·013)	0·860		0·143	(0·130–0·155)
Al		0·020		0·055		1·825	(1·78–1·84)
Cr		0·003		0·017	(0·014–0·019)	0·125	(0·095–0·145)
Na				0·070	(0·063–0·078)		
Ti				0·012	(0·010–0·015)		
Mn				0·024	(0·014–0·035)		
Nor	91·3	92·1		93·6		80·5	
J4	88·2	89·5		90·8		75·5	
Kola	88·2	89·5		90·8		75·5	
Baro	90·5	93·5		94·2		82·5	

463: 40 kb, 1000°C; 173·15 h; H_2O = 2%; ol, opx, cpx, grt; EDS

	ol	*opx*		*cpx*		*grt*	
Ca		0·018	(0·016–0·021)	0·830	(0·820–0·848)	0·141	
Al		0·042	(0·041–0·044)	0·075	(0·074–0·079)	1·860	(1·84–1·865)
Cr		0·006	(0·004–0·008)	0·023	(0·021–0·025)	0·130	(0·125–0·130)
Na				0·075	(0·075–0·085)		
Ti						0·006	(0·000–0·014)
Mn						0·025	
Nor	90·1	91·5		92·5		90·1	
J4	89·4	90·2		90·8		77·8	
Kola	89·4	90·2		90·8		77·8	

451: 41·8 kb, 1100°C; 67·15 h; H_2O = 2%; ol, opx, cpx, grt; EDS

	ol	*opx*		*cpx*		*grt*	
Ca		0·025	(0·023–0·027)	0·820	(0·812–0·822)	0·135	(0·130–0·140)
Al		0·042	(0·038–0·050)	0·061	(0·059–0·065)	1·843	(1·825–1·86)
Cr		0·0064	(0·0054–0·0076)	0·020	(0·018–0·022)	0·130	(0·115–0·145)
Na				0·058	(0·053–0·064)		
Ti						0·017	(0·012–0·022)
Mn						0·021	(0·019–0·024)
Meym	90·6	91·0		91·2		81·5	
Nor	91·0	92·1		92·4		84·0	
J4	90·6	91·0		91·2		81·5	

406: 40 kb, 1200°C; 24·5 h; H_2O = br.%; ol, opx, cpx, grt; EDS

	ol	*opx*		*cpx*		*grt*	
Ca		0·040	(0·038–0·045)	0·760	(0·740–0·780)	0·129	(0·126–0·132)
Al		0·057	(0·054–0·060)	0·073	(0·071–0·076)	1·854	
Cr		0·008	(0·007–0·010)	0·020	(0·018–0·021)	0·135	
Na				0·055	(0·044–0·066)		
Ti						0·011	(0·007–0·015)
Mn						0·015	(0·010–0·020)
SC-1	91·1	91·5		91·4		83·5	
SCS	91·1	91·5		91·4		83·5	
J4	91·1	91·5		91·4		83·3	

TABLE 2 (*Continued*)

459: 40 kb, 1300°C; 18·15 h; H_2O = br.; ol, opx, cpx, grt; EDS							
	ol	*opx*		*cpx*		*grt*	
Ca		0·057	(0·054–0·058)	0·690		0·127	(0·122–0·133)
Al		0·095	(0·093–0·100)	0·110		1·864	
Cr		0·017	(0·011–0·019)	0·020		0·123	
Na				0·058			
Ti						0·013	
Mn						0·018	
Nor	90·4	90·4		89·0		83·2	
Meym	89·9	90·5		89·5		84·2	
J4	89·4	90·0				83·1	
347: 50 kb, 900°C; 255 h; H_2O = 5%; ol, opx, cpx, grt; WDS							
	ol	*opx*		*cpx*		*grt*	
Ca		0·011		0·885		0·150	(0·144–0·157)
Al		0·016	(0·016–0·022)	0·043		1·805	
Cr		0·004	(0·004–0·007)	0·017		0·125	(0·110–0·145)
Na		0·0016	(0·0012–0·0021)	0·050	(0·030–0·060)		
Ti		0·0017	(0·001–0·0025)	0·002		0·024	
Mn						0·016	
Baro	91·3	93·0		94·5		86·5	
SC-1	90·9	91·5		93·5		79·0	
SCS	90·9	91·5		93·5		79·0	
J4	90·9	91·5		93·5		79·0	
462: 50 kb, 1000°C; 161 h; H_2O = 5%; ol, opx, cpx, grt; EDS							
	ol	*opx*		*cpx*		*grt*	
Ca		0·014	(0·012–0·016)	0·830	(0·820–0·840)	0·135	(0·129–0·140)
Al		0·025	(0·023–0·027)	0·065		1·850	(1·81–1·86)
Cr		0·004	(0·000–0·006)	0·020	(0·015–0·030)	0·130	(0·100–0·150)
Na				0·080	(0·070–0·100)		
Ti						0·015	
Mn						0·020	
Nor	91·2	92·3		93·2		82·8	
J4	90·4	91·3		92·2		79·0	
Kola	90·4	91·3		92·2		79·0	

249: 50 kb, 1100°C; 60 h; $H_2O = 2\%$; ol, opx, cpx, grt; WDS

	ol	opx	cpx		grt	
Ca		0·021	0·840	(0·820–0·855)	0·130	(0·133–0·137)
Al		0·028	0·041	(0·038–0·048)	1·843	(1·79–1·90)
Cr		0·0045	0·0036	(0·0026–0·0044)	0·130	(0·075–0·140)
Na		0·003	0·034	(0·028–0·054)		
Ti		0·0021	0·0036	(0·0026–0·0044)	0·024	(0·016–0·032)
Mn					0·015	(0·010–0·018)
SC-1	90·6	92·0	92·3		80·8	
J4	90·6	92·0	92·3		80·8	
SCS	90·6	92·0	92·3		80·8	

320: 50 kb, 1200°C; 16·75 h; H_2O = abs.; ol, opx, cpx, grt; WDS

	ol	opx	cpx		grt	
Ca		0·032	0·790	(0·050–0·056)	0·120	(0·115–0·150)
Al		0·038	0·052	(0·011–0·014)	1·805	
Cr		0·0058	0·012	(0·030–0·050)	0·130	
Na		0·005	0·040	(0·001–0·0026)		
Ti		0·0012	0·0018		0·017	(0·008–0·026)
Mn					0·017	(0·014–0·021)
Baro	91·4	92·8	93·0		86·0	
SC-1	90·7	90·5	91·2		82·0	
SCS	90·7	90·5	91·2		82·0	

407: 50 kb, 1300°C; 4·5 h; H_2O = abs.; ol, opx, cpx, grt; EDS

	ol	opx	cpx		grt	
Ca		0·044	0·680	(0·081–0·098)	0·125*	(0·119–0·128)
Al		0·052	0·084	(0·013–0·018)	1·830	(1·815–1·83)
Cr		0·008	0·014	(0·066–0·096)	0·125	
Na			0·070*			
Ti					0·018	(0·015–0·022)
Mn					0·015	(0·013–0·016)
J4	89·8	91·1	90·5		83·0	
SC-1	89·8	91·1	90·5		83·0	

TABLE 2 (*Continued*)

248: 50 kb, 1400°C; 24 h; H_2O=abs.; ol, opx, cpx, grt; WDS							
	ol	*opx*		*cpx*		*grt*	
Ca		0·070	0·540	0·118			
Al		0·080	0·105	1·830			
Cr		0·009	0·016	0·110			
Na		0·010	0·050				
Ti		0·001	0·001	0·011			
Mn				0·0105			
Baro	92·1	92·5	91·6	87·7			
408: 60 kb, 1300°C; 0·75 h; H_2O=abs.; ol, opx, cpx, grt; EDS							
	ol	*opx*		*cpx*		*grt*	
Ca		0·040	(0·028–0·058)	0·710	(0·688–0·732)	0·124*	(0·107–0·138)
Al		0·037	(0·035–0·040)	0·075	(0·073–0·082)	1·820	(1·80–1·83)
Cr		0·006	(0·003–0·008)	0·016	(0·015–0·017)	0·125	(0·115–0·130)
Na				0·089*	(0·082–0·096)		
Ti						0·026*	(0·026–0·037)
Mn						0·016	(0·014–0·018)
J4	89·7	91·0		90·8		82·5	
SC-1	89·7	91·0		90·8		82·5	
418: 60 kb, 1300°C; 6 h; H_2O=abs.; ol, opx, cpx, grt; EDS							
	ol	*opx*		*cpx*		*grt*	
Ca		0·037	(0·034–0·039)	0·700	(0·660–0·710)	0·124*	(0·121–0·127)
Al		0·039	(0·035–0·044)	0·075	(0·071–0·085)	1·820	(1·80–1·83)
Cr		0·006	(0·005–0·007)	0·016	(0·012–0·019)	0·125	(0·115–0·130)
Na				0·080	(0·072–0·089)		
Ti						0·022*	(0·016–0·028)
Mn						0·020	(0·016–0·024)
J4	90·5	91·3		90·8		82·3	
SC-1	90·5	91·3		90·8		82·3	

419: 60 kb, 1400°C; 4 h; H_2O = abs.; ol, opx, cpx, grt; EDS

	ol	*opx*		*cpx*		*grt*	
Ca		0·057	(0·053–0·060)	0·620	(0·600–0·640)	0·117*	(0·116–0·125)
Al		0·051	(0·048–0·053)	0·080	(0·069–0·091)	1·810	
Cr		0·007	(0·006–0·008)	0·015	(0·012–0·019)	0·125	(0·115–0·130)
Na				0·076	(0·058–0·094)		
Ti						0·015	
Mn						0·017	(0·014–0·019)
J4	89·5	90·3		89·1		83·3	
SC-1	89·5	90·3		89·1		83·3	

The values for Ti, Al, Cr, V, Mn, and Ca are given as cation proportions in the structural formula based on six oxygens for orthopyroxene and clinopyroxene, on 32 oxygens for spinel and on 12 for garnet [NB: Ca for garnet denotes Ca = Ca/(Ca + Mg + Fe)]. Values in parentheses give width of experimental brackets; *denotes compositional gap. Mg and Fe are given as *mg*-numbers for minerals from the various starting materials. They can be found in line with the names of starting materials in columns headed with the mineral names. Run number (P denotes piston cylinder), pressure, temperature, run time, H_2O added (wt.%, br = breathed on samples, abs. = absorbed water), run products and mode of microprobe analysis (EDS = energy dispersive, WDS = wavelength dispersive) are given in the first lines of each run.

the Bi I–II, Tl I–II, Ba I–II, and Bi III–IV transitions and, at high temperatures, with the silver melting curve (Mirwald & Kennedy, 1979), the quartz–coesite transition (Mirwald & Masonne, 1980), and the graphite–diamond boundary (Kennedy & Kennedy, 1976). The three reaction boundaries were corrected in the above studies for the effect of pressure on the emf of the thermocouple, and thus our calibration empirically includes this correction. Temperatures were measured with a $Pt_{94}Rh_6/Pt_{70}Rh_{30}$ thermocouple both in the piston cylinder and in the belt apparatus. Details of the calibration procedure were given by Brey *et al.* (in press), who found an accuracy for temperature of ± 7 °C and for pressure of $\pm$(1% nominal pressure +0·5 kb), comparable to that given by Mirwald *et al.* (1975) for piston cylinder apparatus.

Water was added to charges in amounts (relative to amount of starting material) given in the headings for individual runs in Table 2. Lower-temperature experiments contained more water than those from higher temperatures. Absorbed water was present for runs at any temperature because we stored the starting materials in closed glass vials in the atmosphere of our laboratory. In our initial experiments we added 10% water or more for low-temperature experiments (below solidus) to ensure reaction. This was very successful, and all clinopyroxene was reacted out by dissolution of various components into the coexisting fluid phase. The fluid phase was probably distributed in cracks and pores all over the olivine capsules and effectively transported chemical components away from the charges. These experiments are not reported in this study.

After quenching, the Pt cylinders with the olivine capsules were cut perpendicularly at half length, embedded in epoxy resin, and polished. Major elements were measured in the energy-dispersive mode (EDS), using a CAMECA microprobe (CAMEBAX Microbeam) with an attached Si (Li) detector (KEVEX) at the Institut für Geowissenschaften, Universität Mainz. The accelerating voltage was 15 kV, the beam current 20 nA and the counting time 100 s. ZAF correction procedures are after Reed & Ware (1975), who also gave the detection limits of their procedure. We have tested our calibration with the set of reference samples for electron microprobe analysis as published by Jarosewich *et al.* (1980). Several experiments were also measured in the wavelength-dispersive mode (WDS) with 15 kV acceleration voltage and a beam current of 6 nA (the mode of measurement is indicated in Table 2 by EDS and WDS).

Phases to be analysed with the electron microprobe were selected on back-scattered electron images which clearly distinguish between olivine (ol) and orthopyroxene (opx) (dark) and clinopyroxene (cpx) and garnet (grt) (light). Superimposed X-ray intensity images for Al further helped to distinguish between ol and opx and between cpx and grt.

STARTING MATERIALS

The demonstration of true equilibrium in experimental studies is very difficult, even in the simplest systems, as metastable equilibria can produce homogeneous run products or be reversed like stable equilibria. In chemically simple systems, criteria established by Schreinemaker's rules can be used to help in the interpretation of experimental run products. This is no longer possible in complex systems, and strict reversals become impractical (Perkins & Newton, 1980). It is therefore prudent when working with natural systems to select only a few well-defined starting materials which approach equilibrium from different chemical 'directions'. Equilibrium compositions should lie in the region of chemical overlap of the microprobe analyses. Starting materials used here were a synthetic mineral mix, mixes of mineral separates from natural garnet and spinel lherzolites and a sintered oxide mix. The bulk compositions (A)–(D) matched that of spinel lherzolite SC-1 of

Jagoutz *et al.* (1979), which is believed to represent a primitive mantle composition (Table 1), but more clinopyroxene-rich compositions have also been used (see below).

(A) Synthetic mineral mix 'Baro'

This consists of a complex garnet synthesized at 40 kb and 1150 °C from gel (Table 1), an enstatite synthesized at 1 atm and 1250 °C from gel, chemically pure (p.a.) Na_2CO_3, and a natural olivine [Mo22—see Preß *et al.* (1986) and Table 1] mixed to match the composition of SC-1 as closely as possible. Only the *mg*-number (92) is higher than in SC-1 (89·7). Garnets approach equilibrium from high Ca, Ti, Cr, and Mn, and low Fe contents. Orthopyroxene has to take in all other elements except Mg and Si, and cpx has to nucleate from opx and grt. Olivine loses Fe to the other phases during the experiment.

(B) Mineral mix 'SC-1'

Handpicked mineral separates (ol, opx, cpx, sp) of spinel lherzolite SC-1 (Jagoutz *et al.*, 1979) were ground, sieved to $>20\ \mu m$, and remixed in the proportions appropriate to SC-1. The mineral analyses given in Table 1 are taken from Blum (1982). Pressure and temperature of crystallization of SC-1 are 12·7 kb and 1052 °C, as calculated from the Ca content of olivine (Köhler, 1989; Köhler & Brey, in press) and the composition of coexisting opx and cpx with our new thermometer (see Part II). Experimental conditions are such that the pyroxenes always lose Al, Cr, Ti, and Na, and increase or decrease their Ca content and *mg*-numbers. Garnet has to nucleate either by unmixing from the pyroxenes or the reaction between pyroxenes and spinel. The Fo content of olivine is mostly a function of bulk composition, and changes only very little.

(C) Mineral mix 'J4'

Magnetic separates of opx-, cpx-, and grt-porphyroblasts (courtesy E. Jagoutz) from a sheared garnet lherzolite nodule J4 (Jagersfontein) were handpicked, ground, sieved to $<20\ \mu m$, and recombined together with J4 olivine in initial experiments and later with olivine ($Fo_{89·5}$) from spinel lherzolite Mog 32 (courtesy D. Ionov) to match SC-1 composition. Representative analyses are given in Table 1. Pressure and temperature of crystallization calculated with our newly developed barometer and thermometer (see Part II) are 58·3 kb and 1354 °C. Garnets are zoned with respect to Ti only (0·58 wt.% $<$ TiO_2 $<$ 1·01 wt.%), whereas pyroxene porphyroblasts appear to be unzoned. Depending on P, T conditions, both opx and cpx lose or gain Al, Cr, and Ca when adjusting to experimental conditions, but always lose Na and Ti. Cr/(Cr + Al) in the garnets always remains about constant, Ca always increases, and Ti decreases. Spinel readily nucleates from the phases present (and garnet did not remain as a residual phase in such experiments), but was always too small to be analysed.

(D) Oxide mix 'SCS'

Fired reagent-grade oxides (SiO_2, TiO_2, Al_2O_3, Cr_2O_3, MnO, NiO, and MgO) and carbonates ($CaCO_3$ and Na_2CO_3) were sintered at 800 °C for several hours, finely ground, and mixed with synthetic fayalite to match the composition of SC-1. All phases except olivine have to nucleate from the sinter products.

In conjunction with a project on the solubility of Ca in olivine as a function of pressure and temperature (Köhler, 1989; Köhler & Brey, in prep.), three further starting materials [(E)–(G)] were used which consisted of hand-picked, ground, and sieved ($<20\ \mu m$) opx, cpx, and spinel from spinel lherzolite Mo22 (Tariat, Mongolia; Preß *et al.*, 1986) remixed with different olivines in approximate proportions (wt.%) of ol:opx:cpx:sp = 40:30:28:2. The higher proportions of cpx was chosen to ensure its presence at any P, T conditions even when there was a large amount of fluid phase or melt present. Mineral analyses given in Table 1 are from Preß *et al.* (1986) and from Köhler (1989). Pressure and temperature of

crystallization of Mo22 are 21·8 kb and 1132 °C, and were calculated as for SC-1. Reaction directions of minerals during the experiment are very similar to those for SC-1. Mo22 pyroxenes and spinel were mixed with the following olivines:

(E) Spinel lherzolite 'Nor'

Olivine (Fo_{93}) from a dunite in Ålesund (Norway); bulk Mg value is increased compared with SC-1.

(F) Spinel lherzolite 'Kola'

Olivine ($Fo_{86\cdot5}$) from an olivine–magnetite–perovskite cumulate from Lesnaya Varaka complex (Kola Peninsula); bulk Mg value is very similar to SC-1.

(G) Spinel lherzolite 'Meym'

Zoned olivines (Fo_{86-89}) from a meymechite (Meymecha–Kotui district, Siberia; courtesy L. Kogarko); bulk Mg value is very similar to SC-1.

ADJUSTMENT TO EQUILIBRIUM

Olivine

Five to 10 olivine grains were usually analysed for major elements in each charge after the experiment. Grain-sizes for olivines and all other phases range from 5 to 30 μm, depending on the type of starting material (smaller for synthetic mixtures), temperature (larger for higher T), and the presence (larger) or absence (smaller) of melt or fluid phase (mostly H_2O). Olivine seems to reach equilibrium during experimental run times as the variation of Fo content in all experiments lies within $\pm 0{\cdot}3$ (1σ) of the value given in Table 2. This is in accordance with the fast diffusion rates of elements in olivine (e.g., Morioka, 1981; Jurewicz & Watson, 1988). Ca contents in olivine were determined in a separate detailed investigation and are published elsewhere (Köhler & Brey, in press).

Orthopyroxene

About 10 orthopyroxenes were usually analysed after the experiments in each of the starting materials, and the region of compositional overlap between the run products from the various starting materials was inferred as the equilibrium value. Only analyses with a structural formula total (based on six oxygens) between 3·99 and 4·01 were accepted. The orthopyroxenes are generally zoned with compositions near equilibrium at the rims and less-reacted compositions in the cores. The zonation gives approximately linear correlation trends between the elements (Fig. 3a–c) even at 900 °C. The element variation diagrams allow us to define equilibrium mineral compositions rather tightly from intersecting straight lines: there are P, T conditions (e.g., Fig. 3a) where opx from the spinel lherzolites has to release Al (to form garnet), whereas opx from the garnet lherzolite takes in Al (to consume garnet). Ca, Mg, Fe, and Cr react concomitantly in trying to reach equilibrium. Experimental brackets are established clearly in cases with opposite reaction directions. At other P, T conditions orthopyroxenes from both garnet and spinel lherzolite starting materials have to give off Al or Al may remain constant (Fig. 3b and c). Despite this, equilibrium compositions can be established unequivocally because element correlation lines usually intersect obliquely. Figure 3b also demonstrates that orthopyroxenes from starting material Nor adjust to high *mg*-numbers as a result of high bulk *mg*-number. The linear correlation between *mg*-number and Al shows that Fe–Mg adjustment and the nucleation and growth of garnets are simultaneous processes. The higher *mg*-number should cause higher Ca in

opx and lower Ca in cpx [see Davidson & Lindsley (1985) for a comprehensive overview] but the deviations found are within analytical error, so that the same Ca contents were assigned to the pyroxenes from starting materials with high and low *mg*-numbers. The sintered oxide mix SCS yields pyroxene compositions which cluster around equilibrium compositions (Fig. 3c) but the correlation lines from the crystalline starting materials more tightly constrain equilibrium compositions.

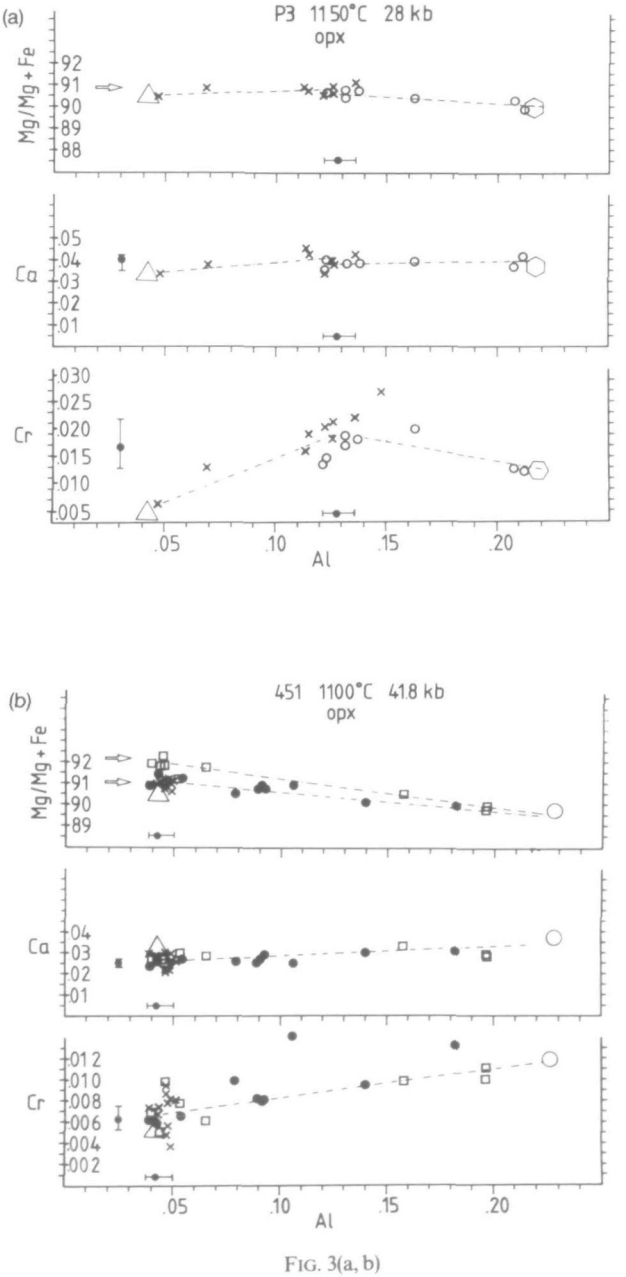

FIG. 3(a, b)

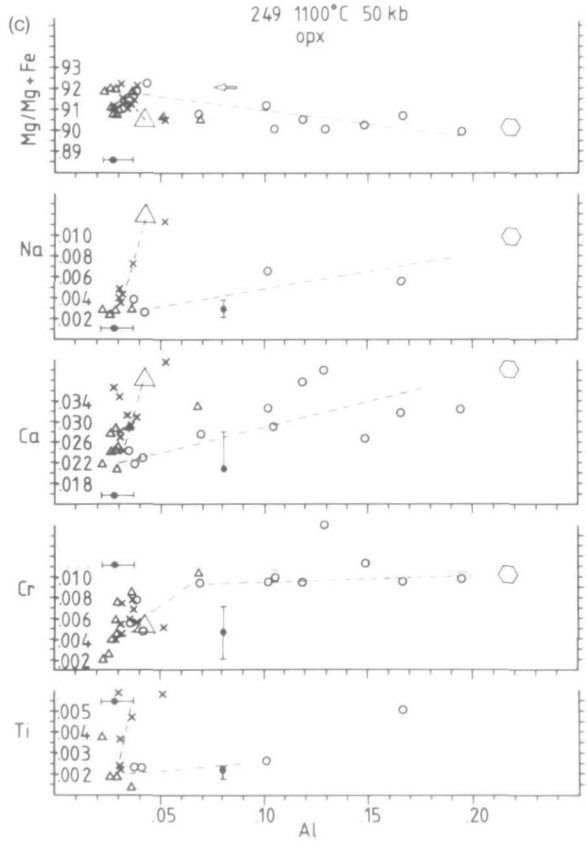

FIG. 3. Diagrams showing adjustment of orthopyroxene compositions from the various starting materials (dash–dot lines) to experimental conditions and demonstrating method of evaluation of equilibrium compositions by overlap of reaction trends. Equilibrium compositions were evaluated with diagrams of *mg*-number, Na, Ca, Cr, and Ti (proportions of cation in structural formula based on six oxygens) vs. Al. Three examples from different *P*, *T* conditions are shown here. Small symbols indicate reaction products in different starting materials: × = J4, open circles = SC-1, open squares = Nor, open triangles = SCS; closed circles = Meym. Large symbols show original mineral compositions in these starting materials: triangles = J4, hexagons = SC-1, circles = Mo22. Bars: region of compositional overlap; dots and arrows: selected values. (a) *28 kb and 1150 °C*. Orthopyroxenes from grt lherzolite starting material J4 (×) react to higher Al, Ca, and Cr contents and slightly higher *mg*-numbers. Orthopyroxenes from sp lherzolite starting material SC-1 (open circles) react to higher Cr contents and somewhat higher *mg*-numbers, whereas Ca remains constant and Al decreases. We have taken the compositional overlap as the experimental bracket and used the midpoints for further processing. These values and the width of the brackets are given in Table 2. (b) *41·8 kb and 1100 °C*. J4 orthopyroxenes practically do not change their composition, because of a coincidence whereby the lower pressure and temperature of the experiment give the same composition as at the higher pressure and temperature of this nodule. SC-1 orthopyroxenes (open circles) also react towards this composition and fully overlap with J4 orthopyroxenes. Opx from a second spinel lherzolite starting material 'Nor' (open squares) with a somewhat higher bulk *mg*-number than SC-1 but otherwise very similar composition (see Table 1; caused by the addition of an Fo-rich olivine) reacts to higher *mg*-numbers, but very similar Ca, Cr, and Al contents. Experimental brackets are again as indicated. (c) *50 kb and 1100 °C*. Minerals were analysed in the wavelength-dispersive mode (WDS), which gives lower detection limits, for instance, for Na and Ti. Orthopyroxenes from both J4 and SC-1 release Na, Ca, Cr, and Ti, whereas *mg*-numbers increase slightly. Reaction direction is the same for all elements but equilibrium compositions can be inferred reasonably well because of different slopes of the correlation lines. Compositions of nucleated orthopyroxenes from sintered oxide mix starting material SCS are close to equilibrium.

Clinopyroxene

Ten to 15 analyses were usually carried out for each starting material and the same criteria for acceptance of analyses applied as for opx. Na is lost at all P, T conditions from clinopyroxene and also orthopyroxene (Figs. 3c, 4a–c, and Fig. 9b below) because of its high solubility in a coexisting H_2O-rich fluid phase (Ryabchikov *et al.*, 1982) or silicate melt (where present). Al and Cr can be considered to be present in natural clinopyroxenes as Tschermak's molecules but they are also coupled to Na. This causes higher Al and Cr contents relative to orthopyroxenes at all P, T conditions, whereas in CMAS orthopyroxene may have higher Al than clinopyroxene or vice versa depending on P and T (Nickel *et al.*, 1985). When trying to adjust to experimental conditions, clinopyroxenes from spinel lherzolite starting materials always release Al (Fig. 4a–c), because most experimental pressures are higher than the original crystallization pressures of the natural rocks and because Na is always lost (see above). Al in J4 cpx slightly increases in rare instances (Fig. 4a) or remains constant, but usually decreases (Fig. 4b) even though there are many higher-temperaure and/or lower-pressure conditions than calculated for the crystallization of J4. Again, the loss of Na is responsible for this behaviour. The presence of melt causes somewhat larger uncertainties in reversed Al, Na, and Cr contents (Fig. 4c), which are not buffered by the coexistence of a phase saturated in these elements, and occur in different concentration levels depending on the amount of melt present. Amounts of melt may vary somewhat between the different holes within the same run, and small differences of Al, Cr, and Na exist (Fig. 4c).

Garnet

Si in the structural formula (based on 12 oxygens) was between 2·98 and 3·00 for most of the 10–15 garnet analyses usually taken in each starting material. The sum of cations was mostly between 8·0 and 8·02. Garnets readily grow from spinel lherzolite starting materials, resulting in complete elimination of spinel by the end of the experiment. Their grossular content is rather variable, as can be seen in Fig. 5a. Garnets from grt lherzolite starting material J4 usually retain their initial composition in the core and always react towards more grossular-rich compositions, which usually overlap with garnets grown from spinel lherzolites and the sintered oxide mix SCS (Fig. 5a). The overlap is then taken as the equilibrium bracket of the experiment. This does not constitute a reversal, for it is implicitly assumed that garnet nuclei from spinel lherzolite starting materials are grossular rich and react towards more pyrope-rich equilibrium compositions. Such behaviour would, however, be similar to the behaviour in CMAS when garnets nucleate from glass (Brey *et al.*, 1986). Our assumption is justified in that the initially grossular-rich garnets from starting material Baro also react towards more pyrope-rich compositions (Fig. 5b) and arrive close to, or within, the experimentally established brackets. Also, SCS garnets plot at these compositions (Fig. 5b) so that we consider garnets to be determined by true reversals.

Garnets from J4 starting material reacted very little in some experiments, and it was difficult to obtain good analyses from garnet rims. All analyses, seemingly not influenced by neighbouring grains, plot close to the starting composition (Fig. 5b). We have taken the midpoint of the compositional gap in such cases (indicated in Table 2 by *) for further processing of the data.

J4 and Baro garnets release Ti at all P, T conditions and adjust to compositions coinciding with the Ti content of the Ca-poor garnets from spinel lherzolite starting materials (Fig. 5a and b). If J4 garnets were in equilibrium with all other phases in the

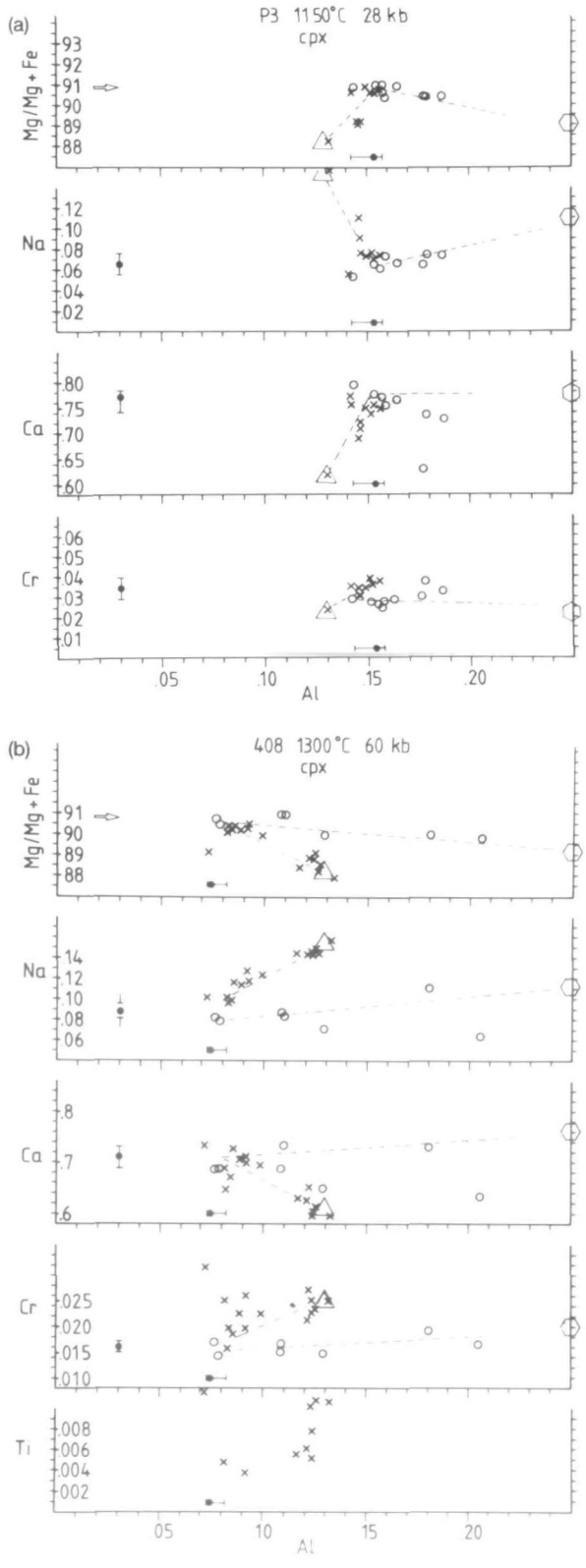

FIG. 4(a, b)

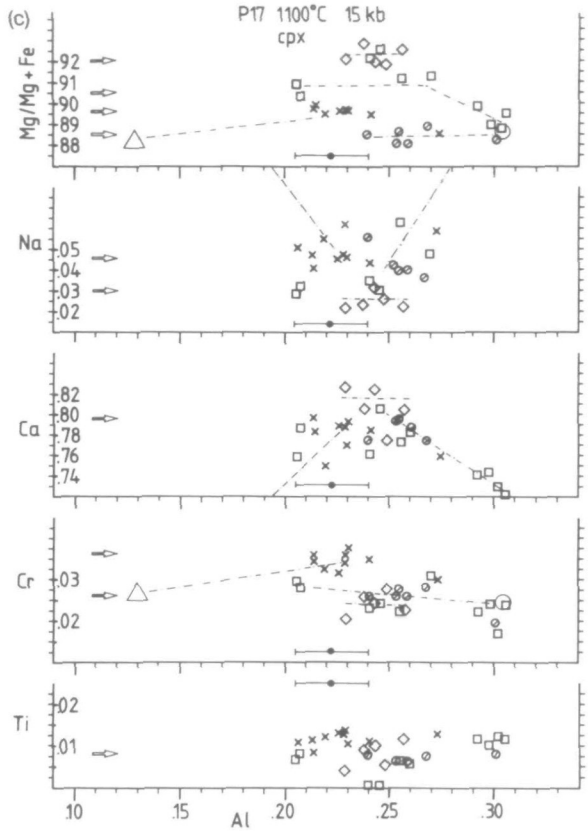

FIG. 4. Examples of adjustment of clinopyroxene composition to experimental conditions. Compositions were evaluated with diagrams of *mg*-number, Na, Ca, Cr, and Ti (proportions of cation in structural formula based on six oxygens) vs. Al. Symbols are as in Fig. 3, and open diamonds = Baro. (a) *28 kb and 1150°C*. *mg*-number, Al, Ca, and Cr in J4 clinopyroxenes increase and Na decreases. In SC-1 clinopyroxenes *mg*-number and Ca increase, whereas Al, Na, and Cr decrease. (b) *60 kb and 1300°C*. These conditions are not far removed from the inferred conditions of origin of garnet lherzolite J4, yet clinopyroxene strongly reacts to higher *mg*-number and Ca content, and to lower Al, Na, Ti, and Cr content. Loss of Na to a coexisting fluid phase causes a decrease in Al and Cr (because of lowered jadeite and ureyite component) and an increase in Ca. *mg*-numbers increase most probably because Fe^{3+} originally present in the starting material was reduced to Fe^{2+} at the low f_{O_2} of our experiments (see text) and this 'excess' Fe^{2+} reacted out of clinopyroxene. Clinopyroxene from SC-1 reacts to very similar compositions. (c) *15 kb and 1100°C*. Melt was present in this experiment and the (small) amounts may have been somewhat different in individual holes. This causes variable Na contents and variable Cr/Al ratios of the clinopyroxenes. The resulting compositional brackets are somewhat wider than in the absence of melt. J4 clinopyroxenes react to Al-, Ca-, Cr-, and Ti-rich compositions and lose Na. Clinopyroxenes (Mo22) from starting materials Kola (circles with bars) and Nor release Na and Al and increase in Ca and Cr. Clinopyroxenes in Nor react to higher *mg*-numbers than those in Kola because of the different *mg*-numbers of the bulk compositions. Clinopyroxenes have to nucleate in synthetic garnet peridotite Baro and react to very similar compositions to those from Nor. Ti is practically identical from all four starting materials.

natural rock sample, Ti should remain constant rather than decrease (as it does) in experiments close to the calculated conditions of crystallization for J4 (58 kb, 1350°C). This discrepancy may be explained by loss of Ti to a coexisting vapour phase.

Mn is always lost from Baro garnets (Fig. 5b) and gained by or lost from J4 garnets, depending mostly on temperature. Garnets from spinel lherzolite Kola (with an Mn-rich

olivine; Table 1) nucleate Mn rich, whereas those from spinel lherzolite Nor, with an Mn-poor olivine (Table 1), are Mn poor at high Ca contents and adjust to Mn contents similar to those from other starting materials close to the inferred experimental bracket (Fig. 5a).

Cr in J4 garnets changes only very little and matches Cr contents of the garnets from spinel lherzolite starting materials, SCS, and Baro (Fig. 5a and b).

Al tends to remain lower in reacted J4 garnets than in those from the other starting materials and thus large experimental brackets for Al result. The reason for the lower Al contents is possibly the loss of Ti from the octahedral positions in garnet which have to be filled mostly by Al. This is indicated by a linear correlation of Ti with Al at almost constant Cr in the zoned garnets of starting material J4 (compare Fig. 10 h below). Experimental run times may be too short to allow filling of the vacant positions left by Ti with Al. In trying to establish equilibrium compositions we therefore do not use the midpoint of the experimental bracket but rather calculate the Al content of garnet from $Al = 2 - Cr - Ti$. This gives values similar to Al contents of garnets nucleated from the spinel lherzolite starting materials.

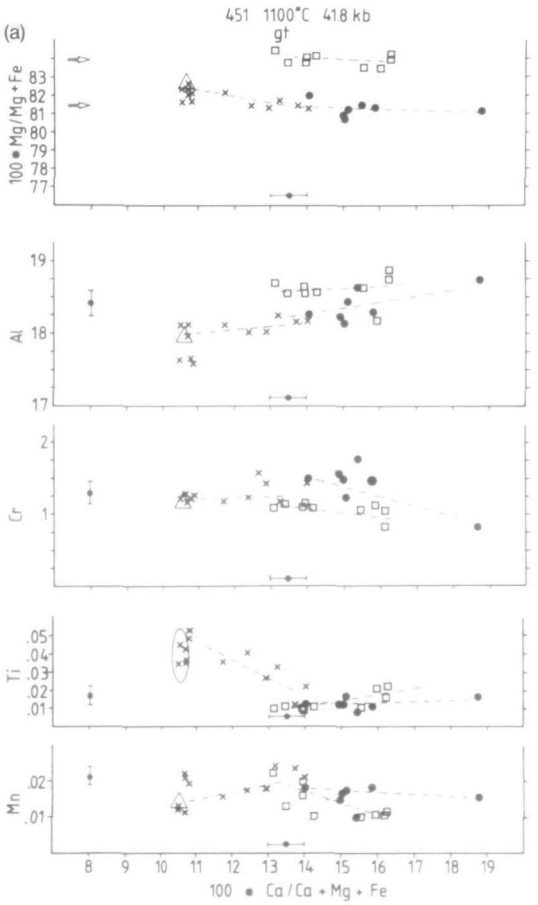

FIG. 5a

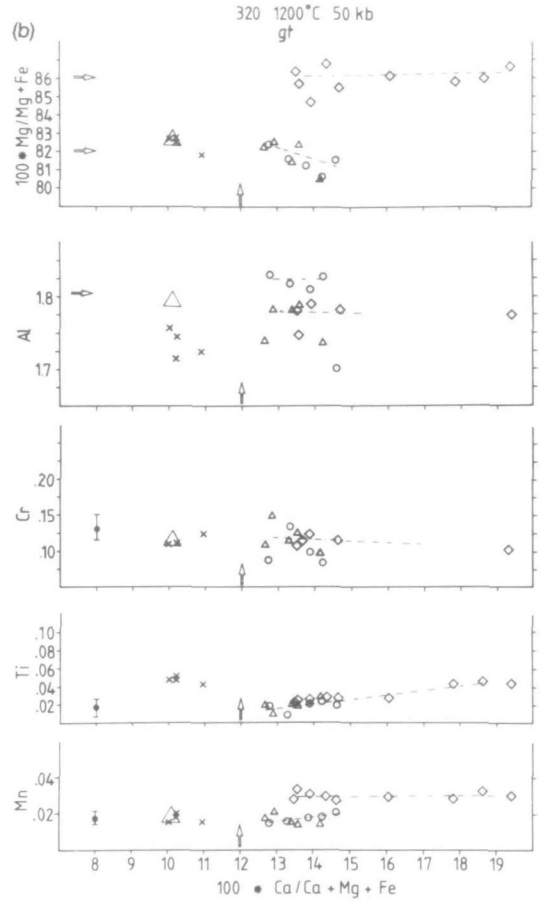

FIG. 5. Adjustment of garnet composition to experimental conditions. Garnet compositions were evaluated with diagrams of *mg*-number, Al, Cr, Ti, and Mn (proportions of cation in structural formula based on 12 oxygens) vs. Ca/(Ca + Mg + Fe). (a) *41·8 kb and 1100°C*. Original compositions are preserved in the cores of J4 garnets (×), whereas the rims and small garnet grains become richer in Ca and Mn, and lower in Ti and *mg*-number. The zoning in Al, Ti (indicated as ellipsoid), and Mn in the Ca-poor cores is the original zoning from the starting material. Garnets have to nucleate in the spinel lherzolite starting materials Meym (filled circles) and Nor (open squares). Meym garnets show a compositional overlap with reacted J4 garnets for all elements, whereas Nor garnets have higher *mg*-numbers and Al, and lower Cr contents. The Ca ratio is similar. Equilibrium brackets were derived from the overlap in composition of J4 and Meym garnets and for the Ca ratio also from Nor garnets. (b) *50 kb and 1200°C*. J4 garnets (×) reacted only very little and there is a gap in Ca ratio to garnets nucleated from SC-1 (open circles) and SCS (triangles) and reacted garnets (from Ca-rich to Ca-poor) from Baro (diamonds). Al, Cr, and Ti overlap in garnets of the last three starting materials, whereas *mg*-number and Mn are higher for Baro garnets. Experimental brackets were defined from the gap in the Ca ratio and from the overlap in composition of J4, SC-1, and SCS garnets.

Spinel

Spinel nucleates readily from J4 and Baro starting materials in experiments at 10 and 20 kb. All garnet is consumed by the end of an experiment. Grain-sizes are typically $< 5\ \mu m$ so that only few good analyses were obtained; these are shown in Fig. 6 and a few are given in Table 3. Experimentally produced spinels from all starting materials are only slightly zoned and probably have reacted close to their equilibrium composition. Melt is always present in these low-pressure experiments in varying amounts (see below), which causes the

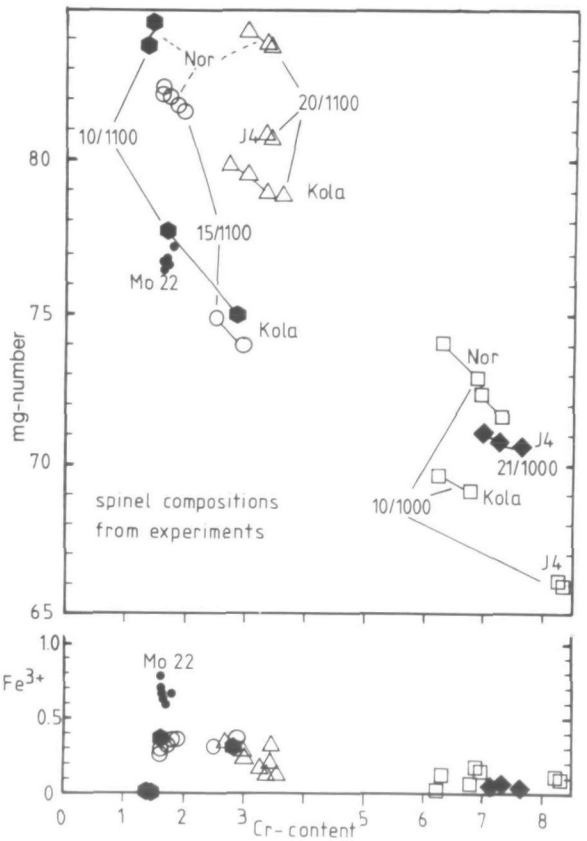

FIG. 6. Composition of spinels produced at different experimental conditions in diagrams of *mg*-number (before calculation of Fe^{3+}) vs. Cr (cation proportion in structural formula based on 32 oxygens) and Fe^{3+} (calculated by assuming 24 cations in the structural formula) vs. Cr. Dots represent our microprobe analyses of spinel from spinel lherzolite Mo22. This spinel was added to all starting materials shown here except for J4, from which spinel had to nucleate. Spinels produced in charges with high *mg*-numbers also have high *mg*-numbers and vice versa. Variable and high Cr contents are caused by the presence of varying amounts of melt.

TABLE 3

Spinel analyses (in wt.% normalized to 100) used to calculate prevailing oxygen fugacities in experiments at different P, T *conditions with the methods of O'Neill & Wall (1987; OW87)*

SiO_2	—	0·35	—	0·13	—
TiO_2	0·44	0·14	0·18	0·59	—
Al_2O_3	32·78	51·12	52·80	30·48	48·22
V_2O_3	0·24	—	—	0·24	—
Cr_2O_3	37·06	16·87	15·10	39·33	21·25
FeO	13·33	11·74	11·92	12·23	9·61
MnO	—	—	—	0·38	—
MgO	16·13	19·76	19·90	16·61	20·32
P, *T*	10/1000	10/1100	15/1100	21/1000	20/1100
log f_{O_2}—QFM: OW87	−5·2	−2·1	−2·1	−5·1	−3·5

observed increase of Cr in spinel. The increase of Cr in spinel, in turn, shifts the garnet-in boundary to higher pressures, which explains the absence of garnet in the 20-kb experiments. The decrease in Fe^{3+} calculated from microprobe analyses by assuming perfect stoichiometry and 24 oxygens in the formula unit must be caused by low oxygen fugacity during the experiment. Oxygen fugacities calculated with the method of Ryabchikov *et al.* (1986) and O'Neill & Wall (1987) give values at around the Fe–FeO buffer (Table 3), indicating the near-absence of Fe^{3+} in our experiments. The reason for low oxygen fugacities in the experiments may be similar to the tentative explanation by O'Neill & Wall (1987) for the difference of oxygen fugacities calculated with their method for spinel lherzolites and the much lower 'intrinsic' oxygen fugacity measurements of Arculus & Delano (1981, p. 1187): 'the ubiquitous presence of a reducing film of organic matter . . . may be responsible for near instantaneous reduction . . . until the nearest self-buffering equilibrium is reached; this, for a Ni-containing phase, may be the appropriate nickel precipitation curve for that phase'. The nickel precipitation curve for mantle olivines with typically 2500–3500 ppm lies very close to the iron–wüstite (IW) buffer which is -4 to -5 log f_{O_2} units below quartz–fayalite–magnetite (QFM) (O'Neill & Wall, 1987). Use of single-crystal mantle olivines from San Carlos as sample containers for our experiments appears to buffer oxygen fugacity at low values by this effect.

Melt

Melt is present in all experiments between 10 and 21 kb where small amounts of water were added to promote reaction. It can be identified with back-scattered electron images as interstitial pockets of quench crystals between and overgrowth onto larger primary crystals. The quench crystals are mostly clinopyroxenes with more Fe- and Al-rich compositions than equilibrium clinopyroxenes. The amount of melt was not determined.

EXPERIMENTAL RESULTS

Experimental results and run details are given in Table 2 and shown in Figs. 6–10. The *mg*-numbers of minerals in these figures (and as discussed below) are taken from a combination of experimental results of starting materials J4, SC-1, SCS, Meym, and Kola, all of which have very similar bulk Mg/(Mg + Fe) ratios. The *mg*-numbers of the minerals were combined with the preferred values from the brackets for other elements (Table 2) as derived from element or element ratio variation diagrams such as Figs. 3–5. Si was not evaluated from variation diagrams but was calculated using the preferred values for other elements and assuming stoichiometry and absence of Fe^{3+}.

The data in Table 2 are brackets and preferred values from all starting compositions derived from element variation diagrams in the manner explained in Figs. 3–6. The full set of diagrams (based on ~3000 mineral analyses) and a computer listing of the preferred mineral compositions for all experimental conditions can be obtained from the senior author on request.

Olivine

Forsterite contents (Fo) in olivine range from 87·6 to 91·5 (Fig. 7). This range is larger than the analytical error and the compositional variation in individual runs. Fo content in olivines changes with the amount of melt present, which explains the variations in the experiments from 10 to 21·2 kb. For other runs there is a tendency for the Fo content in

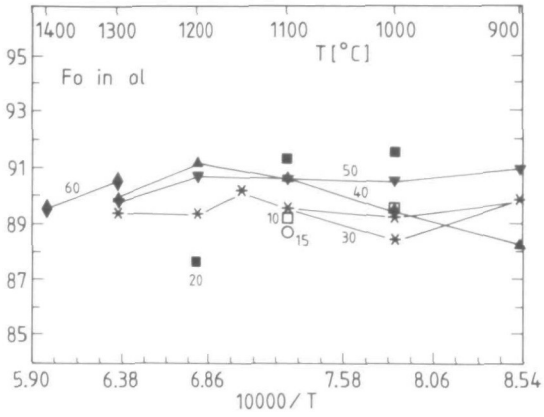

FIG. 7. Fo content in olivine plotted against reciprocal temperature. Numbers beside the lines in the graphs are pressures in kb and the symbols indicate equal experimental pressure. Fo in olivine is not dependent on temperature but tends to increase with pressure in the experiments from 30 to 60 kb (two runs at 28 kb are included with the 30-kb symbols in this and all following figures). Irregular variation of Fo in olivine is caused by varying amounts of melt in runs at lower *P*.

olivine to increase with increasing pressure, as seen in Fig. 7 (see also Part II), but no temperature dependence is observed.

Orthopyroxene

The *mg*-numbers in orthopyroxenes vary between 88·4 and 92, a range very similar to that found in the olivines. Also, similarly, there is possibly an increase of *mg*-number with pressure but no change with temperature (Fig. 8a). The lack of temperature dependence is in accordance with earlier work on the distribution of Fe and Mg between olivine and orthopyroxene (e.g., Medaris, 1969; Sack, 1980), which indicates equilibrium in our experiments with respect to partitioning of Fe and Mg between coexisting minerals.

The natural logarithm of Ca content of orthopyroxene increases linearly with increasing temperature at constant pressure and decreases linearly with increasing pressure at constant temperature (Fig. 8b). The dashed lines in this figure are lines fitted to the Ca contents of opx in the simple CMS system [values taken from Nickel & Brey (1984)]. They are a very good fit to our natural system experiments.

Al content in orthopyroxene is solely a function of temperature in the spinel lherzolite facies as shown, for example, by Gasparik (1984) and Sen (1985) for CMAS. Our experiments also seem to indicate a slight pressure dependence (Fig. 8c), but this may be an artefact caused by the presence of melt. Al has a higher preference for melt than Cr and this causes a decrease in the Al/Cr ratio of the residual orthopyroxenes. This is shown, for example, by Al in opx from the experiment at 20 kb, 1200 °C (higher amount of melt) being lower than at 20 kb, 1100 °C, and vice versa for Cr (compare Fig. 8c and d).

Al content is a function of both pressure and temperature in the garnet lherzolite facies (Fig. 8c) and has been the basis of a widely used barometer since it was first calibrated by MacGregor (1974) in the simple MAS system. Isotherms of Al in opx from reversed experiments in MAS by Perkins *et al.* (1981) have a steeper slope and lie at higher Al contents than those seen from our experiments in Fig. 8c. Uncertainty exists about appropriate corrections needed to relate simple-system experiments to natural rocks.

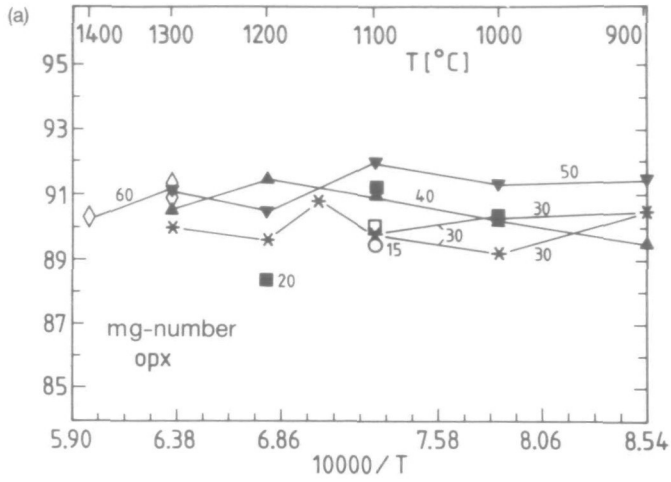

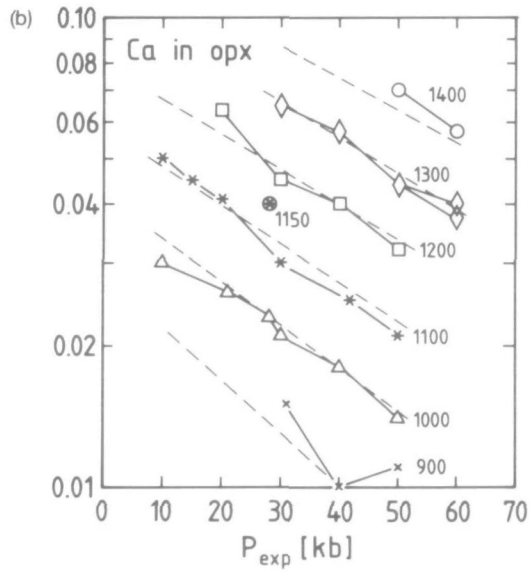

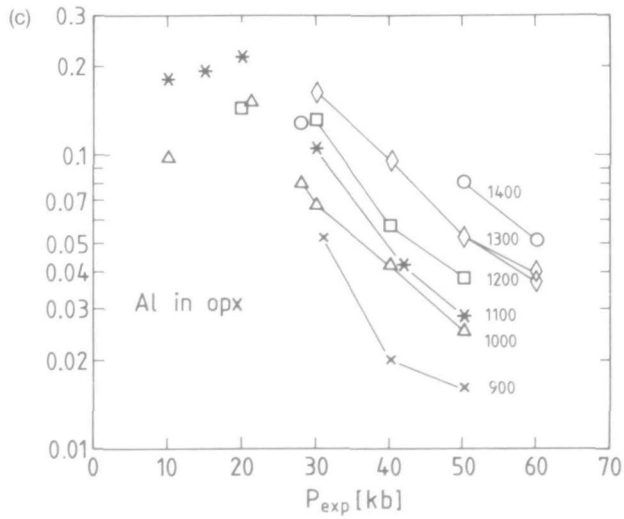

FIG. 8(a–c)

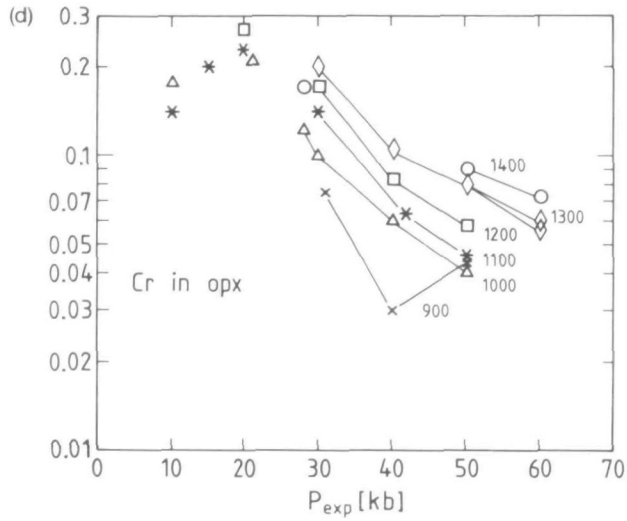

FIG. 8. Variation of orthopyroxene compositions (given as cations in structural formula based on six oxygens) with pressure and temperature. Symbols and numbers as in Fig. 7. (a) *mg*-numbers in orthopyroxene do not depend on temperature but tend to increase with pressure at $P_{exp} \geq 28$ kb, as in olivine. (b) Ca content of orthopyroxene plotted on a logarithmic scale vs. pressure. It can be seen that ln Ca depends linearly on pressure and temperature. Numbers denote experimental temperatures in °C and isothermal experiments are shown by the same symbols. The broken lines are isotherms calculated from a least-squares fit of Ca content of orthopyroxenes from the simple CMS system (see formula in Part II). The agreement with the results from the complex system is striking. (c) Al in orthopyroxene for spinel- and garnet-bearing assemblages plotted on a logarithmic scale against pressure. Numbers and symbols as for (b). Al decreases with increasing pressure and decreasing temperature in the garnet lherzolite facies. A slight curvature of isotherms may be indicated. In the spinel-bearing assemblage it is mostly a function of temperature, but the Al/Cr ratio is also a function of the amount of melt which is present in our experiments. This can be seen from the experiments at 20 kb, where the 1200°C experiment has a lower Al content than that at 1100°C but a higher Cr content (Fig. 8d). (d) Cr in orthopyroxene for spinel- and garnet-bearing assemblages plotted on a logarithmic scale against pressure. Cr decreases with increasing pressure and decreasing temperature in the garnet lherzolite facies, as does Al, and isotherms are curved. Cr contents become very low at low temperatures and analytical errors were accordingly higher, which may be the reason for the high Cr in the experiment at 50 kb, 900°C. Cr in opx appears somewhat erratic in experiments in the spinel field, also probably because of the presence of varying amounts of melt.

Cr in opx also increases with increasing temperature and decreases with increasing pressure in the garnet stability field (Fig. 8d). The dependence of Cr in opx on pressure decreases with increasing pressure, as seen by the curvature of isotherms in Fig. 8d. Cr in opx may also be usable as a barometer, as suggested by Webb & Wood (1986) and Nickel (1989), but will be more difficult to handle because of the lower content of Cr compared with Al (by a factor of 10) and the lack of sufficient experimental data in other, simpler systems [only data in the system CMASCr exist, and from a very restricted pressure range—Nickel (1989)].

Clinopyroxene

The *mg*-numbers in clinopyroxene increase with decreasing temperature and tend to increase with pressure in those experiments without melt (Fig. 9a). The exchange of Fe and Mg between cpx and ol or opx may be the basis for a thermometer, as shown by Mori & Green (1978).

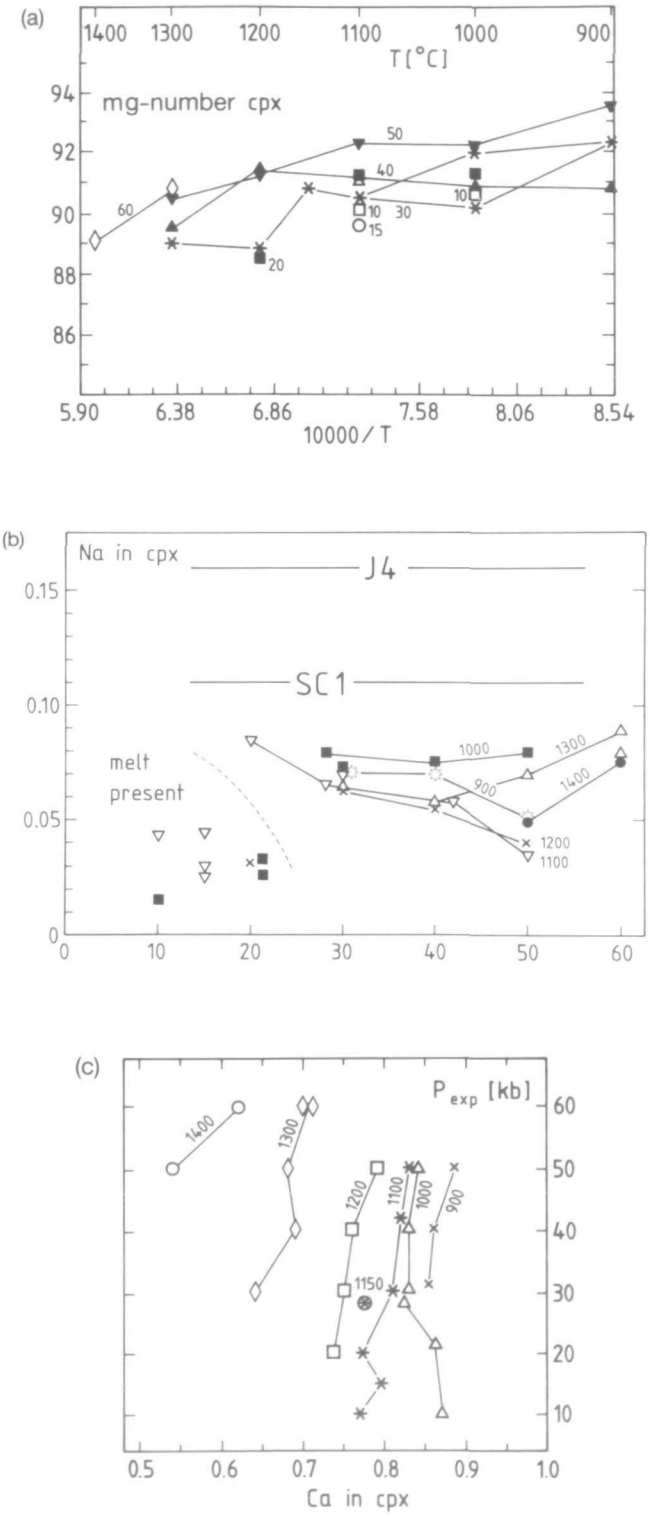

FIG. 9(a–c)

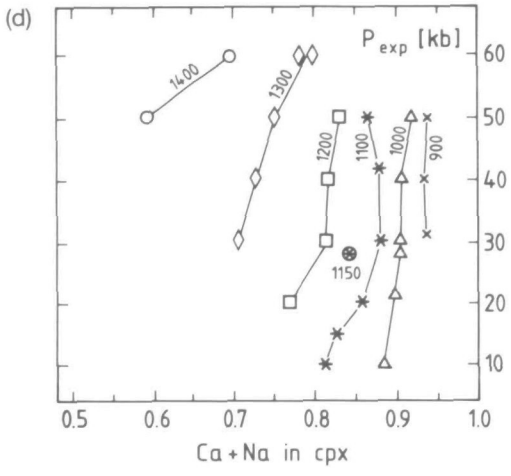

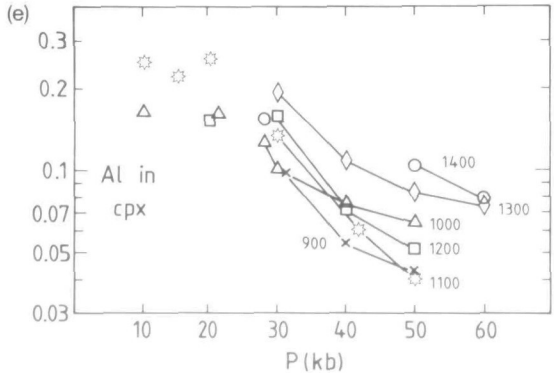

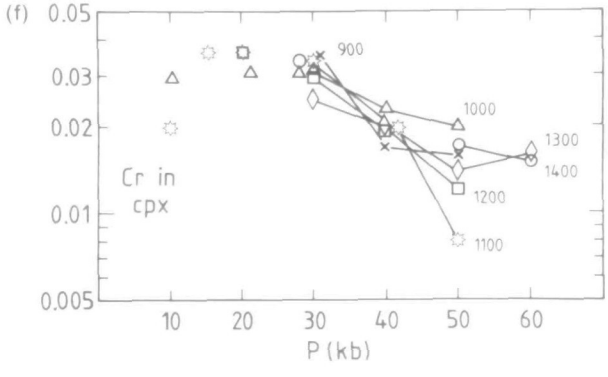

FIG. 9(d–f)

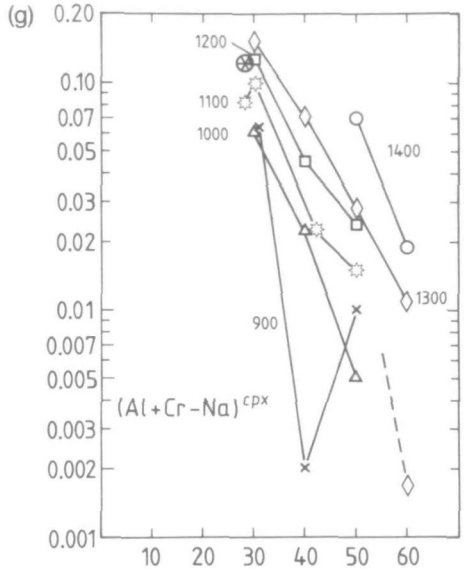

FIG. 9. Variation of clinopyroxene compositions (given as cations in structural formula based on six oxygens) with pressure and temperature. (a) *mg*-number in clinopyroxene as a function of reciprocal temperature. Curve labels and symbols as in Fig. 7. *mg*-numbers in clinopyroxene increase with decreasing temperature and also tend to increase with pressure at $P \geqslant 28$ kb, as in olivine and orthopyroxene. (b) Na content in experimentally produced clinopyroxenes and clinopyroxenes of starting materials J4 and SC-1. Na is always released from clinopyroxenes during an experiment at any P, T condition because of either partitioning into a melt or a fluid phase. (c) Ca content in clinopyroxene as a function of pressure and temperature. There is considerable overlap of Ca between the 900–1100 °C experiments which seemingly excludes the use of the diopside component in clinopyroxene as a precise thermometer. (d) Ca + Na in clinopyroxene as a function of pressure and temperature. Other than for Ca alone [see (c)] the 900–1100 °C isotherms are clearly separated. This shows the possibility of designing a reasonably precise thermometer from these data when an appropriate Na correction is applied. (e) Al in clinopyroxene as a function of pressure and temperature. As in opx, Al seems to be a function of temperature only in the spinel stability field, but its concentration is also influenced by the presence of small amounts of melt in our experiments. Al decreases with increasing pressure and decreasing temperature in experiments in the garnet stability field; however, the 900 and 1000 °C isotherms crosscut the 1100 and 1200 °C isotherms. This is caused by the higher Na content of clinopyroxenes from these experiments [compare (b)]. (f) Cr in clinopyroxene as a function of pressure and temperature. Cr decreases with increasing pressure in the garnet stability field, but the isotherms crosscut each other so that no temperature dependence is recognizable. This irregular behaviour resembles the irregular Na content in (b), and it seems that the presence of Na has a more pronounced effect on Cr than on Al. For the same reason, and because of the presence of melt, Cr in clinopyroxenes from the spinel stability field also is somewhat erratic. (g) $[(Al + Cr) - Na]^{cpx}$ can be considered to reflect the tschermakitic component in clinopyroxene. In contrast to (e) and (f), isotherms from 1000 to 1400 °C are clearly separated and $[(Al + Cr) - Na)]^{cpx}$ shows a pronounced pressure dependence. The experiments at 900 °C do not conform to this; which may be because of combined errors from analysis and the evaluation in the element variation diagrams.

Na contents are always lower in experimentally produced clinopyroxenes than in those from the starting materials (Fig. 9b). Low partition coefficients with melt or hydrous fluids (Ryabchikov *et al.*, 1982) cause the drastic decrease. Na is lowest in clinopyroxenes in the low-pressure experiments where melt is present. Small but varying amounts of water were added to the experiments at lower temperatures (see Table 2), and Na partitioned into this fluid phase. Small amounts of fluids were present also in the higher-temperature experiments from fluid inclusions in olivine and from H_2O absorbed in the starting materials.

The diopside component (reflected by the Ca content) of clinopyroxene is the basis of the widely used two-pyroxene thermometer (Davis & Boyd, 1966). Ca contents of our experimentally produced clinopyroxenes clearly depend on temperature (Fig. 9c) but the data

shown in this diagram are too erratic (at least at lower temperatures) to serve as the basis for a precise thermometer. Rather smooth curves result when Na is added to Ca, and the isotherms are separated very clearly (Fig. 9d). The profound influence of Na on Ca solubility in clinopyroxene has been recognized earlier (Wood & Banno, 1973; Bertrand & Mercier, 1985), but our experiments provide the first opportunity to test suggested correction procedures. As shown for CMS by Nickel & Brey (1984) the pressure dependence of (Ca + Na) decreases with increasing pressure but increases with increasing temperature (Fig. 9d).

In garnet-bearing runs, Al content in clinopyroxene decreases with increasing pressure and decreasing temperature in experiments at $\geqslant$1100 °C, but the 900 and 1000°C isotherms cut across those from higher temperatures (Fig. 9e). Cr also decreases with increasing pressure, but a temperature dependence is not discernible (Fig. 9f). The amount of Al and Cr in clinopyroxene is correlated with the amount of Na. However, Na is rather variable in the experimentally produced clinopyroxenes (Fig. 9b) because of the presence of uncontrolled amounts of melt and fluid phase, and Al and Cr should therefore also vary irregularly. This is especially the case for Cr (Compare Fig. 9e and f) and, because of this, we argue for a stronger influence of Na on Cr than on Al. When Na is subtracted from (Al + Cr) and plotted on a logarithmic scale against pressure (Fig. 9g), a linear, temperature-dependent relationship is obtained. In this procedure only 'tschermakitic' Al and Cr are considered in this way, which could be the basis for a further geobarometer.

Garnet

The *mg*-numbers in garnets increase with increasing temperature and tend to decrease with increasing pressure (Fig. 10a). The temperature dependence is the net result of a strong increase of Mg with temperature (Fig. 10b) and a less-pronounced decrease of Fe (Fig. 10c). In this respect, garnet is the counterpart for olivine, orthopyroxene, and clinopyroxene. The exchange of Fe and Mg between these phases and garnet can be used for thermometry (Ellis & Green, 1979; O'Neill & Wood, 1979; Harley, 1984).

Mn content in garnet is apparently a function of temperature only, and the influence of pressure cannot be resolved with our analytical data. If the one experiment at 50 kb and 900 °C is not considered there seems to be a curvilinear decrease of Mn with increasing temperature (Fig. 10d).

Ca contents in garnet depend (at constant Cr content) on pressure and temperature (Fig. 10e). The influence of pressure decreases strongly at higher pressures, whereas there is a linear dependence on temperature. This is in contrast to the results from CMAS, where Ca decreases linearly with increasing pressure and is practically independent of temperature (Brey *et al.*, 1986). The difference in composition between CMAS and natural rock systems is mostly the presence of Fe and Cr in the latter, and cross-site interactions of Fe–Cr and Ca–Cr must be responsible for the behaviour of Ca in complex garnets.

The variation of Cr in garnet lies within the width of the experimental brackets (Fig. 10f) except for one outlier at 1150 °C. Midpoints of brackets for the 40-, 50- and 60-kb experiments coincide whereas those for the 30-kb experiments are somewhat lower. If real, such variation with pressure mirrors the behaviour of Ca (Fig. 10d), where the 30-kb isobar is clearly separated from the 40-, 50- and 60-kb isobars, which are only very slightly different. In general, Cr in garnet is almost the same at all P, T conditions and merely reflects the bulk Cr content of the rock.

Al in garnet seems to depend slightly on pressure (Fig. 10g) and out of necessity on Ti, as it was evaluated by calculating Al = 2 − Cr − Ti and Cr is practically constant at all

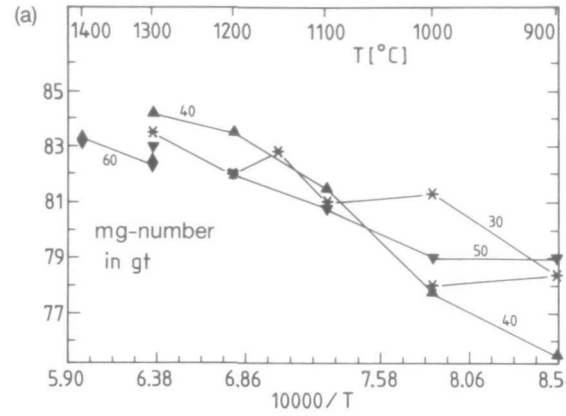

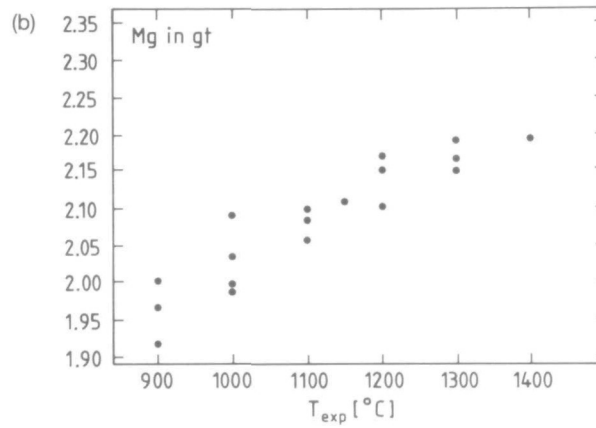

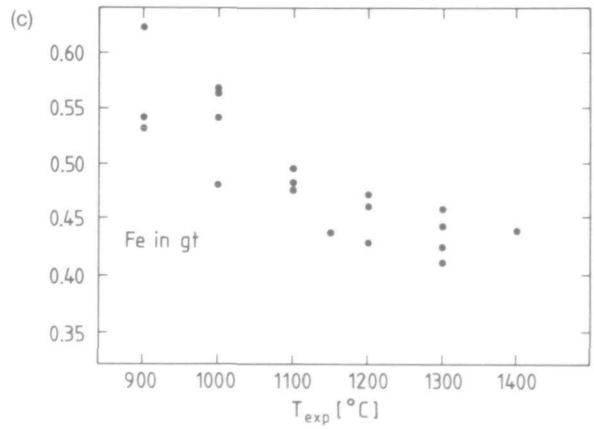

FIG. 10(a–c)

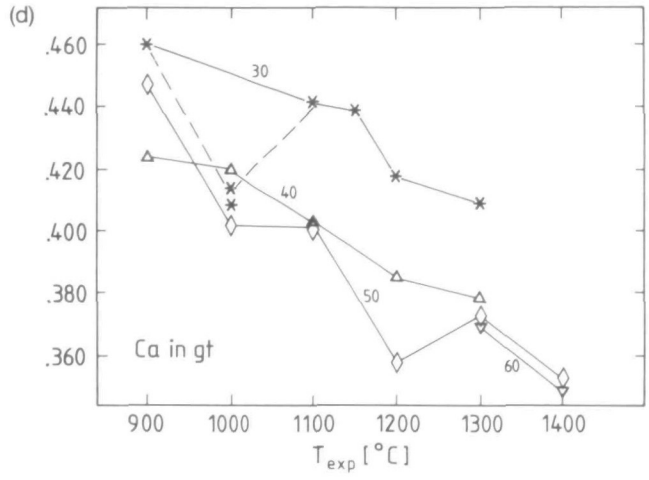

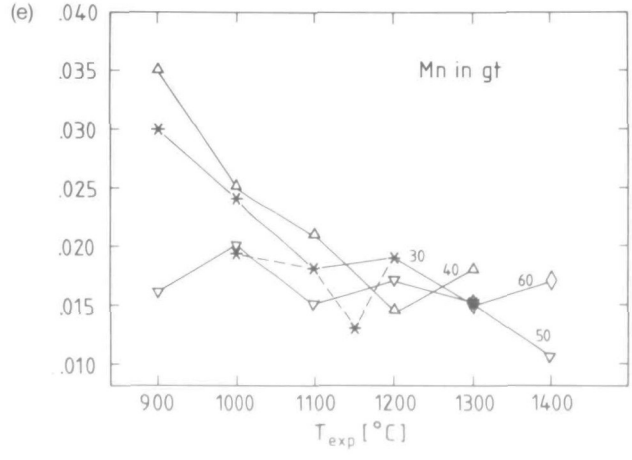

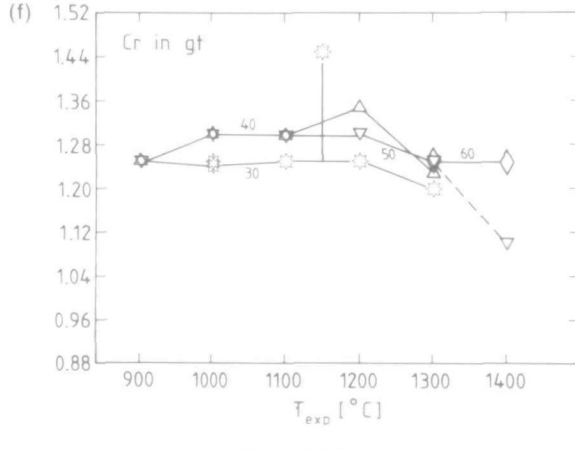

FIG. 10(d–f).

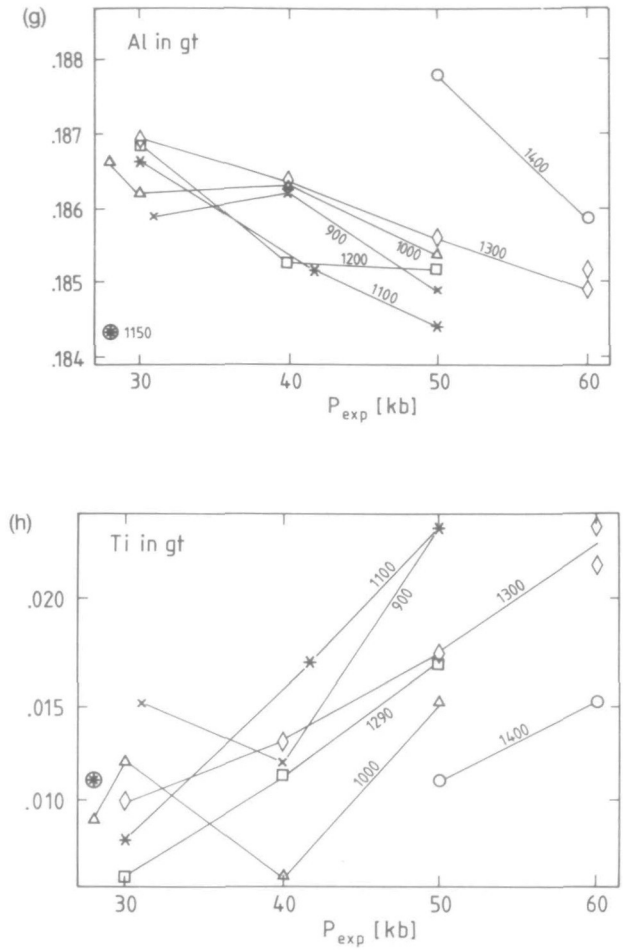

FIG. 10. Variation of garnet compositions (given as cations in structural formula based on 12 oxygens) with pressure and temperature. (a) *mg*-number in garnet as a function of reciprocal temperature and pressure (values in kb). *mg*-numbers in garnet decrease with decreasing temperature and also tend to decrease with increasing pressure, and thus behave in a complementary fashion to olivine, orthopyroxene, and clinopyroxene. (b) The increase of *mg*-numbers with temperature is the net result of a strong increase of Mg with temperature and (c) a weaker decrease of Fe in garnet with temperature. (d) Mn in garnet as a function of temperature. It seems to be a logarithmic function, but only when the experiment at 900 °C, 50 kb is neglected. (e) Ca in garnet decreases linearly with increasing temperature. A decrease with pressure is most pronounced between 30 and 40 kb, above which the influence of pressure almost disappears. (f) Cr in garnet appears to be independent of pressure and temperature and reflects only the bulk composition. Garnets from the 30-kb experiments may contain somewhat less Cr than those from higher pressures. There is a good reason for the one outlier at 30 kb. (g) Al in garnet decreases with increasing pressure with no discernible dependence on temperature. The values shown here are calculated from Al = 2 − Cr − Ti. (h) Ti contents in garnet increase with increasing pressure, although the apparent increase is only slightly larger than the width of the compositional bracket.

pressures and temperatures. Ti content in garnet should therefore also be pressure dependent, which seems to be the case (Fig. 10h). A dependence on temperature cannot be discerned in Fig. 10g and h. The picture may be blurred by solubility of Ti in a coexisting H_2O-rich fluid phase, which lowers the Ti content of garnets (and also pyroxenes), depending on the amount of vapour phase present (Ti is not buffered by a coexisting Ti-saturated phase). Such solubility was, however, not indicated by the experiments of

Schneider & Eggler (1986) and Tatsumi *et al.* (1986). Nevertheless, Ti disappears during experiments because it is always lower in the experimentally produced garnets and pyroxenes compared with those from J4 starting material. We cannot decide upon this question because of lack of detailed information on the H_2O contents of the experiments.

FINAL REMARKS

The experimental results presented in this paper offer the unique possibility for simultaneous testing of many different thermobarometers, which have been based on different exchange reactions and calibrated in many different laboratories. All of these thermobarometers have to reproduce our experimental conditions (within the stated errors) if (1) pressure and temperature calibrations of experimental apparatus are consistent between the various laboratories, and (2) extrapolation from simple-system experiments and in pressure and temperature are correct. Errors in P, T calibration and incorrect compositional extrapolations should mostly cause systematic offsets, whereas erroneous extrapolations of P and T should cause deviations outside the experimental range. Any suitable thermometers and barometers from the literature, and any new thermometers designed from the present data, can then be applied simultaneously to natural rocks, allowing us to derive P, T conditions more accurately and to find possible disequilibria effects. This is the object of Part II of this series.

REFERENCES

Akella, J., 1976. Garnet pyroxene equilibria in the system $CaSiO_3$–$MgSiO_3$–Al_2O_3 and in a natural mineral mixture. *Am. Miner.* **61**, 589–98.

Arculus, R. J., & Delano, J. W., 1981. Intrinsic oxygen fugacity measurements: techniques and results for spinels from upper mantle peridotite and megacryst assemblages. *Geochim. Cosmochim. Acta* **45**, 899–913.

Bertrand, P., & Mercier, J.-C. C., 1985. The mutual solubility of coexisting ortho- and clinopyroxene: toward an absolute geothermometer for the natural system? *Earth Planet. Sci. Lett.* **76**, 109–22.

—— Sotin, C., Mercier, J.-C. C., & Takahashi, E., 1986. From the simplest chemical system to the natural one: garnet peridotite barometry. *Contr. Miner. Petrol.* **93**, 168–78.

Blum, K., 1982. INAA zum Studium der Elementverteilung in den Mineralphasen von Mantelgesteinen. Dissertation, University of Mainz, 1982.

Boyd, F. R., 1973. A pyroxene geotherm. *Geochim. Cosmochim. Acta* **37**, 2533–46.

Brey, G. P., Nickel, K. G., & Kogarko, L., 1986. Garnet–pyroxene equilibria in the system CaO–MgO–Al_2O_3–SiO_2 (CMAS): prospects for simplified ('T-independent') lherzolite barometry and an eclogite-barometer. *Contr. Miner. Petrol.* **92**, 448–55.

—— —— Weber, R., in press. Calibration of a belt apparatus. *J. Geophys. Res.*

Carswell, D. A., & Gibb, F. G. F., 1987*a*. Evaluation of mineral thermometers and barometers applicable to garnet lherzolite assemblages. *Contr. Miner. Petrol.* **95**, 499–511.

—— —— 1987b. Garnet-lherzolite xenoliths in the kimberlites of N Lesotho. *Ibid.* **97**, 473–87.

Davidson, P.M., & Lindsley, D. H., 1985. Thermodynamic analysis of quadrilateral pyroxenes, part II. *Ibid.* **91**, 390–404.

Davis, B. T. C., & Boyd, F. R., 1966. The join $Mg_2Si_2O_6$–$CaMgSi_2O_6$ at 30 kilobars pressure and its application to pyroxenes from kimberlites. *J. Geophys. Res.* **71**, 3567–76.

Dawson, J. B., & Smith, J. V., 1975. Occurrence of diamond in a mica–garnet lherzolite xenolith from kimberlite. *Nature* **254**, 580–1.

Ellis, D. J., & Green , D. H., 1979. An experimental study of the effect of Ca upon garnet–clinopyroxene Fe–Mg exchange equilibria. *Contr. Miner. Petrol.* **71**, 13–22.

Finnerty, A. A., & Boyd, F. R., 1984. Evaluation of thermobarometers for garnet peridotites. *Geochim. Cosmochim. Acta* **48**, 15–27.

—— —— 1987. Thermobarometry for garnet peridotites: basis for determination of thermal and compositional structure of the upper mantle. In: Nixon, P. H. (ed.) *Mantle Xenoliths*. New York: John Wiley.

Gasparik, T., 1984. Two-pyroxene thermobarometry with new experimental data in the system CaO–MgO–Al_2O_3–SiO_2. *Contr. Miner. Petrol.* **87**, 87–97.

Green, D. H., 1973. Conditions of melting of basanite magma from garnet peridotite. *Earth Planet. Sci. Lett.* **17**, 456–65

Harley, S. L., 1984. An experimental study of the partitioning of Fe and Mg between garnet and orthopyroxene. *Contr. Miner. Petrol.* **86**, 359–73.

Jagoutz, E., Palme, H., Baddenhausen, H., Blum, K., Cendales, M., Dreibus, G., Spettel, B., Lorenz, V., & Wänke, H., 1979. The abundance of major, minor and trace elements in the Earth's mantle as derived from primitive ultramafic nodules. *Proc. 10th Lunar Planet. Sci. Conf.*, 2031–50.

Jarosewich, E., Nelen, J. A., & Norberg, J. A., 1980. Reference samples for microprobe analysis. *Geostandards Newslett.* **4**, 43–7.

Jurewicz, A. J. G., & Watson, E. B., 1988. Cations in olivine, Part 2: Diffusion in olivine xenocrysts, with applications to petrology and mineral physics. *Contr. Miner. Petrol.* **99**, 186–201.

Kennedy, C. S., & Kennedy, G. C., 1976. The equilibrium boundary between graphite and diamond. *J. Geophys. Res.* **81**, 2467–70.

Köhler, T., 1989. Der Ca-Gehalt von Olivin im Gleichgewicht mit Clinopyroxen als Geothermobarometer. Dissertation, University of Mainz.

—— Brey, G. P. in press. Ca-exchange between olivine and clinopyroxene as a geothermobarometer calibrated from 2 to 60 kbar in primitive natural lherzolites.

Kushiro, I., Shimizu, N., Nakamura, Y., & Akimoto, S., 1972. Compositions of coexisting liquids and solid phases formed upon melting of natural garnet and spinel lherzolites at high pressures: a preliminary report. *Earth Planet. Sci. Lett.* **14**, 19–25.

MacGregor, I. D., 1974. The system MgO–Al_2O_3–SiO_2: solubility of Al_2O_3 in enstatite for spinel and garnet peridotite compositions. *Am. Miner.* **59**, 110–19.

Medaris, L. G., 1969. Partitioning of Fe^{++} and Mg^{++} between coexisting synthetic olivine and orthopyroxene. *Am. J. Sci.* **267**, 945–68.

Mirwald, P. W., Getting, I. C., & Kennedy, G. C., 1975. Low friction cell for piston-cylinder high-pressure apparatus. *J. Geophys. Res.* **80**, 1519–25.

—— Kennedy, G. C., 1979. The melting curve of gold, silver and copper to 60-kbar pressure: a reinvestigation. *Ibid.* **84**(B12), 6750–6.

—— Masonne, H. J., 1980. The low–high quartz and quartz–coesite transition to 40 kbar between 600 and 1600 °C and some reconnaissance data on the effect of $NaAlO_2$ component on the low quartz–coesite transition. *Ibid.* **85**(B12), 6983–90.

Mori, T., & Green, D. H., 1978. Laboratory duplication of phase equilibria observed in natural garnet lherzolites. *J. Geol.* **86**, 83–97.

Morioka, M., 1981. Cation diffusion in olivine II: Ni–Mg, Mn–Mg, Mg and Ca. *Geochim. Cosmochim. Acta* **45**, 1573–80.

Nickel, K. G., 1983. Petrogenesis of garnet and spinel peridotites. Ph.D. Thesis, University of Tasmania, Hobart.

—— 1989. Garnet–pyroxene equilibria in the system SMACCr (SiO_2–MgO–Al_2O_3–CaO–Cr_2O_3): the Cr-geobarometer. *Proc. 4th Int. Kimberlite Conf.*; *Austr. J. Earth Sci.*

—— Brey, G., 1984. Subsolidus orthopyroxene–clinopyroxene systematics in the system CaO–MgO–SiO_2 to 60 kb: a re-evaluation of the regular solution model. *Contr. Miner. Petrol.* **87**, 35–42.

—— —— Kogarko, L., 1985. Orthopyroxene–clinopyroxene equilibria in the system CaO–MgO–Al_2O_3–SiO_2 (CMAS): new experimental results and implications for two-pyroxene thermometry. *Ibid.* **81**, 44–53.

—— Green, D. H., 1985. Empirical geothermobarometry for garnet peridotites and implications for the nature of the lithosphere, kimberlites and diamonds. *Earth Planet. Sci. Lett.* **73**, 158–70.

Nixon, P, H., & Boyd, F. R., 1973. Petrogenesis of the granular and sheared ultrabasic nodule suite in kimberlites. In: Nixon, P. H. (ed.) *Lesotho Kimberlites*. Maseru: Lesotho National Development Corporation, 67–75.

O'Neill, H. St. C., & Wall, V. J., 1987. The olivine–orthopyroxene–spinel oxygen-geobarometer, the Ni-precipitation curve, and the oxygen fugacity of the Earth's upper mantle. *J. Petrology* **38**, 1169–91.

—— Wood, B. J., 1979. An experimental study of Fe–Mg-partitioning between garnet and olivine and its calibration as a geothermometer. *Contr. Miner. Petrol.* **70**, 59–70.

Perkins, D., III, Holland, T. J. B., & Newton, R. C., 1981. The Al_2O_3 content of enstatite in equilibrium with garnet in the system MgO–Al_2O_3–SiO_2 at 15–40 kbar and 900–1000 °C. *Ibid.* **78**, 99–109.

—— Newton, R. C., 1980. The composition of coexisting pyroxenes and garnets in the system CaO–MgO–Al_2O_3–SiO_2 at 900–1100 °C and high pressures. *Ibid.* **75**, 291–300.

Preß, S., Witt, G., Seck, H. A., Ionov, D., & Kovalenko, V. I., 1986. Spinel peridotite xenoliths from the Tariat Depression, Mongolia, I: major element chemistry and mineralogy of a primitive mantle xenolith suite. *Geochim. Cosmochim. Acta* **50**, 2587–99.

Reed, S. J. B., & Ware, N. G., 1975. Quantitative electron microprobe analysis of silicates using energy-dispersive X-ray spectrometry. *J. Petrology* **16**, 499–519.

Ryabchikov, I. D., Schreyer, W., & Abraham, K., 1982. Compositions of aqueous fluids in equilibrium with pyroxenes and olivines at mantle pressures and temperatures. *Contr. Miner. Petrol.* **79**, 80–4.

—— Ukhanov, A. V., & Ishii, T., 1986. Redox equilibria in upper mantle ultrabasites in the Yakutia kimberlite province. *Geochem. Int.* 38–50.

Sack, R. O., 1980. Some constraints on the thermodynamic mixing properties of Fe–Mg orthopyroxenes and olivines. *Contr. Miner. Petrol.* **71**, 257–69.

Schneider, M. E., & Eggler, D. H., 1986. Fluids in equilibrium with peridotite minerals: implications for mantle metasomatism. *Geochim. Cosmochim. Acta* **50**, 711–24.

Sen, G., 1985. Experimental determination of pyroxene compositions in the system $CaO–MgO–Al_2O_3–SiO_2$ at 900–1200 °C and 10–15 kb using PbO and H_2O fluxes. *Am. Miner.* **70,** 678–95.

Tatsumi, Y. A., Hamilton, D. L., & Nesbitt, R. W., 1986. Chemical characteristics of fluid phase released from a subducted lithosphere and origin of arc magmas: evidence from high pressure experiments and natural rocks. *J. Volcanol. Geotherm. Res.* **29,** 293–309.

Webb, S. A. C., & Wood, B. J., 1986. Spinel–pyroxene–garnet relationships and their dependence on Cr/Al ratio. *Contr. Miner. Petrol.* **92,** 471–80.

Wells, P. R. A., 1977. Pyroxene thermometry in simple and complex systems. *Ibid.* **62,** 129–39.

Wood, B. J., & Banno, S., 1973. Garnet–orthopyroxene and orthopyroxene–clinopyroxene relationships in simple and complex systems. *Ibid.* **42,** 109–24.